The Stability of Plagioclase in the Upper Mantle: Subsolidus Experiments on Fertile and Depleted Lherzolite

GIULIO BORGHINI[1,2]*, PATRIZIA FUMAGALLI[2] AND ELISABETTA RAMPONE[1]

[1]DIPARTIMENTO PER LO STUDIO DEL TERRITORIO E DELLE SUE RISORSE, UNIVERSITÀ DI GENOVA, CORSO EUROPA 26, 16132 GENOVA, ITALY

[2]DIPARTIMENTO DI SCIENZE DELLA TERRA, UNIVERSITÀ DI MILANO, VIA BOTTICELLI 23, 20133 MILANO, ITALY

Plagioclase peridotites are important markers of processes that characterize the petrological and tectonic evolution of the lithospheric mantle in extensional tectonic settings. Studies on equilibrated plagioclase peridotites have documented continuous chemical changes in mantle minerals in response to plagioclase crystallization, potentially tracing the re-equilibration of mantle peridotites up to very low pressure. This experimental study provides new constraints on the stability of plagioclase in mantle peridotites as a function of bulk composition, and the compositional and modal changes in minerals occurring within the plagioclase stability field as a function of P–T–bulk composition. Subsolidus experiments have been performed at pressures ranging from 0·25 to 1·0 GPa, and temperatures ranging from 900 to 1200°C on fertile and depleted anhydrous lherzolites modelled in the system TiO_2–Cr_2O_3–Na_2O–CaO–FeO–MgO–Al_2O_3–SiO_2 (Ti,Cr-NCFMAS). In the fertile lherzolite ($Na_2O/CaO = 0·08$; $X_{Cr} = 0·07$) a plagioclase-bearing assemblage is stable up to 0·7 GPa, 1000°C and 0·8 GPa, 1100°C, whereas in the depleted lherzolite ($Na_2O/CaO = 0·09$; $X_{Cr} = 0·10$) the upper limit of plagioclase stability is shifted to lower pressure. The boundary between plagioclase lherzolite and spinel lherzolite has a positive slope in P–T space. In a complex chemical system, the plagioclase-out boundary is multivariant and sensitive to the X_{Cr} value [$X_{Cr} = Cr/(Cr + Al)$] of spinel. This latter is controlled by the reaction $MgCr_2O_4 + CaAl_2Si_2O_8 = MgCrAlSiO_6 + CaCrAlSiO_6$, which is a function of the Cr–Al partitioning between spinel and pyroxenes, and varies with the X_{Cr} value and chromite/anorthite normative ratio of the bulk composition. Within the plagioclase stability field, the Al content of pyroxenes decreases, coupled with an increase in the anorthite content in plagioclase, and Ti and X_{Cr} in spinel with decreasing pressure; these chemical variations are combined with systematic changes in modal mineralogy governed by a continuous reaction involving both plagioclase and spinel. As a consequence, the composition of plagioclase varies significantly over a rather narrow pressure range and is similar at the same P–T conditions in the investigated bulk-rocks. This suggests the potential application of plagioclase composition as a geobarometer for plagioclase peridotites.

INTRODUCTION

Plagioclase-bearing peridotites occur sporadically in passive continental margin and mid-ocean ridge tectonic settings and represent important geodynamic markers. Their origin can be related either to metamorphic recrystallization at plagioclase-facies conditions or to melt impregnation, and the two processes may imply different thermal histories (i.e. cold vs hot exhumation) of the lithospheric mantle in extensional settings (Müntener & Piccardo, 2003; Müntener *et al.*, 2004; Kazmarek & Müntener,

*Corresponding author. Present address: Dipartimento per lo Studio del Territorio e delle sue Risorse, Università degli Studi di Genova, Corso Europa 26, I-16132 Genova, Italy. Telephone: 0039 10 3538137. Fax: 0039 10 352169. E-mail: giulio.borghini@unige.it

2008). Metamorphic plagioclase-facies recrystallization has been documented in a few plagioclase peridotites from both continental and present-day oceanic settings (Green, 1964; Hamlyn & Bonatti, 1980; Obata, 1980; Kornprobst & Tabit, 1988; Piccardo *et al.*, 1988; Hoogerduijn Strating *et al.*, 1993; Rampone *et al.*, 1993, 2005; Cannat & Seyler, 1995; Ozawa & Takahashi, 1995; Takazawa *et al.*, 1996; Fabries *et al.*, 1998; Furusho & Kanagawa, 1999; Newman *et al.*, 1999; Canil *et al.*, 2003; Chazot *et al.*, 2005; Montanini *et al.*, 2006). In most occurrences, these have been inferred to indicate cold tectonic exhumation of the lithospheric mantle, related to passive extension and thinning of the lithosphere in the early stages of development of an oceanic basin. On the other hand, plagioclase peridotites that originate by melt impregnation have been largely documented in abyssal and ophiolitic peridotites (Menzies, 1973; Dick, 1989; Rampone *et al.*, 1997, 2008; Dijkstra *et al.*, 2001, 2003; Tartarotti *et al.*, 2002; Müntener *et al.*, 2004; Piccardo *et al.*, 2004*a*, 2004*b*, 2005, 2007; Cannat *et al.*, 2006; Borghini *et al.*, 2007; Rampone & Borghini, 2008), and have been related to the diffuse migration, entrapment and crystallization of melts within shallow lithospheric mantle. In many impregnated peridotites, plagioclase is associated with orthopyroxene and/or olivine as a result of melt–rock interaction and, therefore, does not imply the formation of a plagioclase-bearing five-phase mantle assemblage (i.e. plagioclase, olivine, spinel and pyroxenes). Nevertheless, recrystallization concomitant and/or subsequent to melt entrapment may lead to the development of plagioclase-bearing equilibrium textures, thus resulting in equilibration at plagioclase-facies mantle conditions even in impregnated plagioclase peridotites (Takazawa *et al.*, 1996; Rampone *et al.*, 2005; Kazmareck & Müntener, 2008).
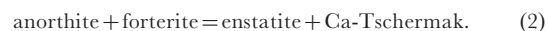
A few of the available studies on equilibrated plagioclase peridotites have documented that the spinel–plagioclase lherzolite transition is indeed a continuous reaction marked by systematic and progressive chemical changes in pyroxenes and spinel, in response to the crystallization of a new Al-bearing phase (Rampone *et al.*, 1993, 2005; Ozawa & Takahashi, 1995; Takazawa *et al.*, 1996; Newman *et al.*, 1999). However, this is poorly supported by parallel experimental investigations, because few studies have so far been performed at subsolidus conditions and in complex chemical compositions approaching those of natural peridotites.

In experimental studies, the stability of plagioclase at upper mantle conditions has been primarily investigated in the simplified chemical system $CaO–MgO–Al_2O_3–SiO_2$, CMAS (Kushiro & Yoder, 1966; MacGregor, 1967; O'Hara, 1967; Obata, 1976; Herzberg, 1978; Gasparik, 1984), where the plagioclase to spinel lherzolite univariant

boundary is the intersection of the strongly *P*-dependent reaction

$$anorthite + forsterite = enstatite + diopside + spinel \qquad (1)$$
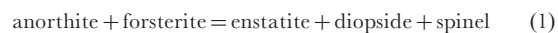
and the *P*- and *T*-dependent reaction

$$anorthite + forterite = enstatite + Ca\text{-}Tschermak. \qquad (2)$$

These studies have shown that the compositions of pyroxenes vary along the univariant plagioclase to spinel boundary, thus defining pyroxene Al-isopleths in both the plagioclase and spinel fields (e.g. Kushiro & Yoder, 1966; Obata, 1976; Herzberg, 1978; Gasparik, 1984).

A series of experimental studies have focused on more complex chemical systems (e.g. CMAS + Na, CMAS + Fe, pyrolite). Most of them have been performed at near-solidus or solidus conditions ($T > 1200°C$), because they addressed mantle partial melting and low-*P* mid-ocean ridge basalt (MORB) generation (e.g. Jaques & Green, 1980; Takahashi, 1986; Falloon & Green, 1987, 1988; Baker & Stolper, 1994; Walter & Presnall, 1994; Baker *et al.*, 1995; Falloon *et al.*, 1997, 1999; Gudfinnsson & Presnall, 2000). These studies indicate that the plagioclase-out boundary occurs at pressures between 1·0 and 1·5 GPa in variably depleted peridotites, suggesting a bulk composition dependence (Green & Falloon, 1998; Falloon *et al.*, 2008). It has also been shown that the addition of Fe, Na and Cr to the CMAS system makes reaction (1) divariant or multivariant if more than one component is added (Green & Hibberson; 1970; Walter & Presnall, 1994; Green & Falloon, 1998; Gudfinnsson & Presnall, 2000; Presnall *et al.*, 2002). In a pioneering paper, Green & Hibberson (1970) explored the subsolidus reactions in the systems forsterite + anorthite, fayalite + anorthite, olivine + labradorite and in a complex pyrolite system, documenting the effect of the addition of pyroxenes on the upper pressure stability of plagioclase. They also demonstrated that the persistence of a five-phase assemblage (plagioclase, spinel, orthopyroxene, clinopyroxene and olivine) in the NCMAS system is bounded at low pressure by reaction (1) and at high pressure by the reaction

$$forsterite + albite = jadeite + enstatite. \qquad (3)$$

Similarly, the addition of Cr to the CMAS system is expected to make reaction (1) divariant, and modify spinel, enstatite and diopside solid solutions, introducing $MgCr_2O_4$ (Mg-chromite), $CaCrAlSiO_6$ (Ca,Cr-Tschermak) and $MgCrAlSiO_6$ (Mg,Cr-Tschermak) end-members. Also, the addition of Cr is thought to expand the stability field of spinel lherzolite (Klemme, 2004), although the transition from plagioclase- to spinel-facies lherzolite in Cr-bearing systems has not yet been investigated by subsolidus experiments.

Experimental studies in complex systems in the subsolidus *P*–*T* space, aimed to define the plagioclase lherzolite

stability field as a function of varying bulk composition, and the chemical changes in mantle minerals as the metamorphic reaction progresses, are still lacking. In this contribution we present the results of subsolidus experiments, performed at pressures ranging from 0·25 to 1·0 GPa and temperatures from 900 to 1200°C, on two different peridotite compositions modeled in the complex system TiO_2–Cr_2O_3–Na_2O–CaO–FeO–MgO–Al_2O_3–SiO_2 (Ti,Cr-NCFMAS). The principal goals of this study are (1) to delimit the subsolidus upper pressure stability of plagioclase under anhydrous conditions in fertile and depleted lherzolite compositions and (2) to define the compositional and modal mineralogical variations as a function of P–T bulk-compositions within the plagioclase stability field, with particular emphasis on the combined effect of Cr and alkalis. Equilibrium element partitioning between coexisting minerals (pyroxenes, plagioclase and Cr-rich spinel) in plagioclase lherzolite assemblages is crucial in assessing the P–T conditions of crystallization of equilibrated plagioclase peridotites, regardless of their subsolidus vs melt-related origin.

EXPERIMENTAL PROCEDURES
Starting materials
Sampling of modern ocean floors and studies on ophiolitic massifs have demonstrated that mantle peridotites with compositions more depleted than typical fertile lherzolites (pyrolite-type composition; Ringwood, 1962) are abundant at extensional settings, as a result of partial melting and/or melt–rock interaction processes (Bodinier & Godard, 2003; Niu, 2004, and references therein). Given this compositional variability, and considering previously investigated model compositions (Green *et al.*, 1979; Jaques & Green, 1980; Falloon & Green, 1987, 1988; Baker & Stolper, 1994; Baker *et al.*, 1995; Falloon *et al.*, 1997, 1999), we focused this study on two peridotite compositions, modelled in the anhydrous complex system TiO_2–Cr_2O_3–Na_2O–CaO–FeO–MgO–Al_2O_3–SiO_2 (Ti,Cr-NCFMAS): (1) a fertile lherzolite (FLZ), and (2) a depleted lherzolite (DLZ). The FLZ composition is an analogue of lherzolite sample ERS2/2 from the Suvero ophiolitic massif (External Liguride Units, Northern Apennine; Rampone *et al.*, 1995), where plagioclase-facies recrystallization has been well documented (Rampone *et al.*, 1993, 1995). It has X_{Mg} = 0·89 [X_{Mg} = Mg/(Mg + Fe^{tot})], X_{Cr} = 0·07 [X_{Cr} = Cr/(Cr + Al)] and an Na_2O/CaO ratio of 0·08 (Table 1). In terms of Al_2O_3 and CaO contents, FLZ is close to previous modelled compositions representative of the MORB source (Fig. 1). This allows direct comparison with previous high-temperature experimental studies (Jaques & Green, 1980; Fallon & Green, 1987, 1988; Baker & Stolper, 1994; Baker *et al.*, 1995; Falloon *et al.*, 1997, 1999). The depleted

lherzolite (DLZ) is similar to the DMM1 composition defined by Wasylenki *et al.* (2003), representing a moderately depleted mantle peridotite after low-degree partial melting. It has slightly higher X_{Mg} (X_{Mg} = 0·90) and X_{Cr} (X_{Cr} = 0·10) and a similar Na_2O/CaO ratio (Na_2O/CaO = 0·09), with respect to FLZ (Table 1). To promote the crystallization of Na-bearing phases, the original DMM1 Na_2O content (0·05 wt %) was increased to 0·20 wt %. Such a value is consistent with the bulk Na_2O contents commonly documented in depleted abyssal peridotites (mostly higher than 0·1 wt %), ascribed to incomplete melt extraction or refertilization by percolating melts and fluids (Elthon, 1992; Niu, 2004). In Table 1 we also report CIPW norms of the investigated bulk-compositions and starting materials from previous experimental studies; this allows us to compare the different bulk compositions in terms of the major end-member mineral components involved in the plagioclase–spinel reactions [e.g. diopside (Di), albite (Ab), anorthite (An), and chromite (Cm)].

To facilitate the identification of minor aluminous phases (plagioclase and spinel), and to increase their modal abundance in the experimental charges, 40% of fosteritic olivine (Fo$_{90}$) was subtracted from the selected compositions (Table 1). The validity of this approach, widely followed in previous experimental studies (e.g. Green & Ringwood, 1970; Jaques & Green, 1980; Niida & Green, 1999), stems from the fact that the expected phase assemblages are oversaturated in olivine.

To promote reaction at the subsolidus temperatures investigated, gels were used as starting materials. They were prepared following the method of Hamilton & Henderson (1968) using tetraethylorthosilicate (TEOS) as the silica source, tetraethylorthotitanate (TEOT) as the titanium source, pure Na-, Ca-, Mg- and Al-nitric solutions, ferric benzoate and ammonium dichromate. Gels were fired in a gas mixing furnace at T = 850°C and fO_2 conditions approaching the FMQ (fayalite–magnetite–quartz) buffer at 1 atm, to ensure that the iron was present in the starting composition dominantly as FeO. Gels were seeded with 1% of a mixture of synthetic pure anorthite (70%) and spinel (30%) to promote the nucleation of the minor phases. Seed compositions largely differ from the expected compositions of corresponding minerals (spinel and plagioclase) stable at the investigated P–T conditions, to allow easy identification of seed relicts. The addition of a seed mixture does not significantly affect the final bulk compositions (Table 1).

Experimental conditions and apparatus
Subsolidus experiments were performed at pressures ranging from 0·25 to 1·0 GPa, and temperatures from 900 to 1200°C (Table 2). To account for the sluggish kinetics in

Table 1: Compositions of starting materials

	1 FLZ	2 FLZ′	3 FLZ″	4 DLZ	5 DLZ′	6 DLZ″	7 OL	8 B. seeds	9 HPY	10 MPY	11 TQ	12 MM3
SiO_2	44·90	47·52	47·35	44·90	47·52	47·35	40·96	30·13	45·20	44·74	45·40	45·50
TiO_2	0·12	0·20	0·20	0·07	0·14	0·14	0·00	0·00	0·71	0·17	0·10	0·11
Cr_2O_3	0·41	0·69	0·68	0·39	0·65	0·64	0·00	0·00	0·43	0·45	0·26	0·68
Al_2O_3	3·79	6·31	6·73	2·38	3·97	4·40	0·00	47·67	3·54	4·37	3·23	3·98
FeO*	7·99	6·96	6·89	8·34	7·54	7·47	9·53	0·00	8·47	7·55	7·61	7·18
MgO	39·12	32·19	31·95	41·58	36·27	35·99	49·51	8·50	37·48	38·57	40·21	38·30
CaO	3·41	5·68	5·77	2·14	3·56	3·67	0·00	13·70	3·08	3·38	3·00	3·57
Na_2O	0·26	0·44	0·44	0·20	0·34	0·34	0·00	0·00	0·57	0·40	0·18	0·31
K_2O	0·00	0·00	0·00	0·00	0·00	0·00	0·00	0·00	0·13	0·00	0·00	0·00
Total	100·00	100·00	100·00	100·00	100·00	100·00	100·00	100·00	99·61	99·63	99·99	99·63
X_{Mg}	0·89	0·89	0·89	0·90	0·90	0·90	0·90	—	0·89	0·90	0·90	0·91
X_{Cr}	0·07	0·07	0·06	0·10	0·10	0·10	—	—	0·08	0·07	0·09	0·10
Na_2O/CaO	0·08	0·08	0·08	0·09	0·09	0·09	—	—	0·19	0·12	0·06	0·09
Mol %												
Ab	0·62	1·07	1·07	0·46	0·77	0·78	—	—	1·39	0·97	0·42	0·73
An	4·94	8·29	8·98	2·89	4·75	5·38	—	—	3·70	5·55	4·17	5·05
Di	4·14	7·03	6·69	2·59	4·23	3·94	—	—	4·70	3·62	3·58	4·39
Hy	22·61	37·77	36·84	25·45	41·61	40·74	—	—	23·39	21·00	26·99	27·48
Ol	67·07	44·79	45·37	68·12	47·79	48·31	—	—	65·03	68·09	64·42	61·49
Il	0·22	0·38	0·38	0·13	0·25	0·25	—	—	1·36	0·32	0·18	0·20
Cm	0·40	0·68	0·68	0·37	0·60	0·60	—	—	0·43	0·45	0·25	0·66
Or	0·00	0·00	0·00	0·00	0·00	0·00	—	—	0·21	0·00	0·00	0·00
Ab/Di	0·15	0·15	0·16	0·18	0·18	0·20	—	—	0·30	0·27	0·12	0·17
Cm/An	0·08	0·08	0·08	0·13	0·13	0·11	—	—	0·12	0·08	0·06	0·13

1FLZ, fertile lherzolite reproducing the composition of peridotites from the External Liguride Units, Northern Apennines (Rampone *et al.*, 1995); 2 FLZ′, fertile lherzolite FLZ minus 40 wt % olivine (Fo_{90}, 7); 3 FLZ″, fertile lherzolite FLZ minus 40 wt % olivine with 1% seed mixture added; 4 DLZ, depleted lherzolite similar to DMM1 (Wasylenki *et al.*, 2003) with Na_2O increased to 0·20 wt %; 5 DLZ′, depleted lherzolite DLZ minus 40 wt % olivine (Fo_{90}, 7); 6 DLZ″, depleted lherzolite DLZ minus 40 wt % olivine with 1% seed mixture added; 7 OL, composition of olivine subtracted from selected bulk compositions; 8 B. seeds, composition of seed mixture composed of 70 wt % pure anorthite and 30 wt % spinel ($MgAl_2O_4$); 9 HPY, 'Hawaiian pyrolite' from Green *et al.* (1979); 10 MPY, 'MORB pyrolite' from Green *et al.* (1979); 11 TQ, 'Tinaquillo peridotite' from Green (1963); 12 MM3, model peridotite from Baker & Stolper (1994). CIPW norms (% mol proportions) are also reported. Ab, albite; An, anorthite; Di, diopside; Hy, hypersthene; Ol, olivine; Il, ilmenite; Cm, chromite; Or, orthoclase.

anhydrous subsolidus systems runs lasted up to 522 h. Experiments at pressures between 0·5 and 1·0 GPa were carried out in a single-stage piston cylinder apparatus at the Dipartimento di Scienze della Terra in Milano (Italy), using a salt–Pyrex–MgO assembly and tapered graphite heater. Temperature was measured by K-type and S-type thermocouples and is considered to be accurate to ±5°C. An initial pressure of 0·25 GPa was applied, then the sample was heated to 400°C to soften the Pyrex and compressed to the final run pressure. A pressure of 0·5 GPa is generally considered as the lower limit of *P* conditions for piston cylinders; therefore, experiments at 0·25–0·31 GPa were conducted in a vertically mounted internally heated pressure vessel at the Bayerisches Geoinstitut (Bayreuth, Germany).

To verify the piston cylinder calibration at 0·5 GPa, the albite + H_2O method (Baker, 2004) was followed. Powder of pure albite plus 15–20 wt % distilled H_2O was loaded into a Pt capsule and run together with the experimental charge at 0·5 GPa and 1100°C (run FLZ-DLZ10). The resulting albite glass was analyzed by wavelength-dispersive electron microprobe (WDS) analysis (beam spot of 20 μm, 15 kV accelerating voltage, 5 nA sample current). Following Baker (2004), the water solubility in the albite glass was determined by difference from the WDS analysis. The result ($H_2O \approx 11.76$ wt %) was compared

with the calibration curve suggested by Baker (2004), indicating a pressure of 0·51 GPa, in agreement with the nominal pressure (0·5 GPa).

Approximately 20 mg of starting material was loaded into a graphite inner capsule (outer diameter 2·8 mm), and then welded into an outer Pt capsule (outer diameter 3·0 mm, length about 7–8 mm). Graphite was used to isolate the sample from the Pt capsule and to avoid Fe loss (Kinzler, 1997; Walter, 1998). The graphite–Pt assembly (combined with preconditioning of the starting material at FMQ) maintained the oxygen fugacity below the graphite–C–O vapor buffer (Ulmer & Luth, 1991).

To maintain anhydrous conditions, the capsule plus the starting material and the assembly were dried in an oven at 250°C for at least 12 h just before welding and running

Fig. 1. MgO vs Al$_2$O$_3$ and CaO (wt %) variation diagrams indicating the bulk compositions used in this study and peridotite starting materials investigated in previous experimental studies (see Table 1): FLZ, fertile lherzolite (this study); DLZ, depleted lherzolite (this study); MM3, peridotite from Baker & Stolper (1994); HPY, Hawaiian pyrolite, and MPY, MORB pyrolite from Green *et al.* (1979); TQ, Tinaquillo peridotite from Green (1963). Also reported are the composition of Primordial Mantle (PM) as given by McDonough & Sun (1995) and the compositional field defined by abyssal peridotites from Niu *et al.* (1997). Black lines correspond to polybaric fractional and batch melting trends at various pressures (kbar) (Niu *et al.*, 1997).

the experiments. Run products were initially characterized by X-ray powder diffraction and inspected using back-scattered electron (BSE) and secondary electron images (using a Philips SEM 515 electron microscope at the Dipartimento per lo Studio del Territorio e delle sue Risorse, University of Genova). Microprobe analyses were performed using a JEOL JXA 8200 Superprobe equipped with five WDS spectrometers and one energy-dispersive spectrometer (EDS) (1 μm beam size; beam conditions 15 kV and 15 nA) at the Dipartimento di Scienze della Terra, University of Milano. Both images and X-ray element maps were extremely useful in textural examination of the experimental charges.

Approach to equilibrium

Demonstration of equilibrium through a reversal experiment is difficult in the case of complex chemical systems and for continuous reactions. Thus, no reversals were performed. However, the approach to equilibrium was
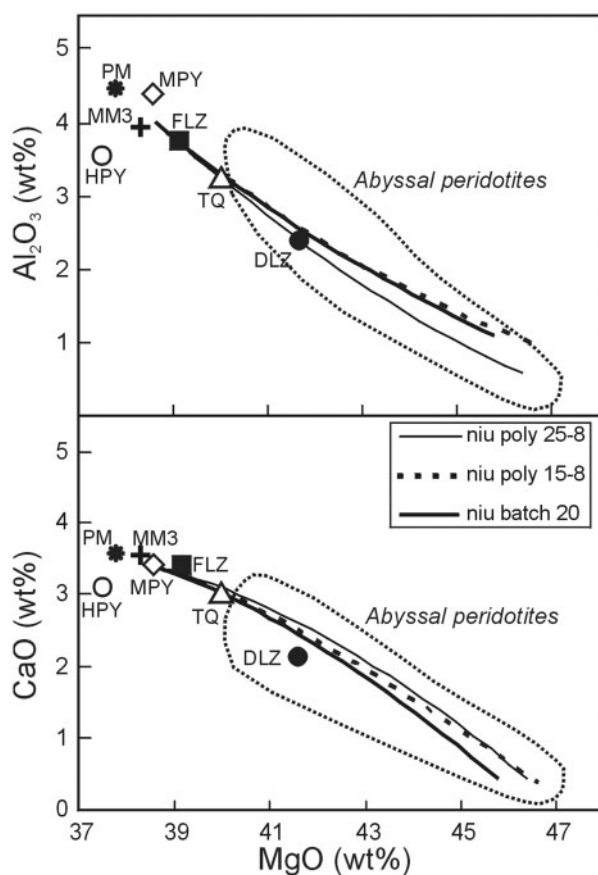
Table 2: Experimental run conditions

Run no.	P (GPa)	T (°C)	t (h)	Apparatus	Run products
FLZ9	0·25	1150	168	IHPV	ol, opx, cpx, glass, sp
FLZ13	0·31	1100	168	IHPV	ol, opx, cpx, pl, sp
FLZ10	0·5	1100	520	SS-PC	ol, opx, cpx, pl, sp
FLZ14	0·6	1000	534	SS-PC	ol, opx, cpx, pl, sp
FLZ3	0·6	1100	308	SS-PC	ol, opx, cpx, pl, sp
FLZ5	0·7	1000	336	SS-PC	ol, opx, cpx, pl, sp
FLZ7	0·7	1150	408	SS-PC	ol, opx, cpx, pl, sp
FLZ0	0·8	900	480	SS-PC	ol*, opx*, cpx*, sp*, amph*
FLZ12	0·8	1000	518	SS-PC	ol, opx, cpx, sp
FLZ2	0·8	1100	377	SS-PC	ol, opx, cpx, pl, sp
FLZ6	0·9	1100	522	SS-PC	ol, opx, cpx, sp
FLZ11	0·9	1200	120	SS-PC	ol, opx, cpx, glass, sp
FLZ4	1·0	1000	288	SS-PC	ol, opx, cpx, sp
FLZ1	1·0	1100	523	SS-PC	ol, opx, cpx, sp, amph
DLZ9	0·25	1150	168	IHPV	ol, opx, cpx, glass, sp
DLZ8	0·27	1100	168	IHPV	ol, opx, cpx, pl, sp
DLZ10	0·5	1100	520	SS-PC	ol, opx, cpx, pl, sp
DLZ14	0·6	1000	534	SS-PC	ol, opx, cpx, pl, sp
DLZ5	0·7	1000	336	SS-PC	ol, opx, cpx, sp
DLZ7	0·7	1150	408	SS-PC	ol, opx, cpx, pl, sp
DLZ12	0·8	1000	518	SS-PC	ol, opx, cpx, sp
DLZ6	0·9	1100	522	SS-PC	ol, opx, cpx, sp

FLZ, fertile lherzolite (= 3 in Table 1); DLZ depleted lherzolite (= 6 in Table 1); ol, olivine; opx, orthopyroxene; cpx, clinopyroxene; sp, spinel; pl, plagioclase; amph, amphibole; IHPV, internally heated pressure vessel; SS-PC single-stage piston cylinder.
*Phases detected only by X-ray powder diffraction technique.

carefully assessed through the following observations: (1) the growth of compositionally homogeneous, chemically unzoned minerals, probably enhanced by the long duration of the experimental runs (Table 2); (2) systematic and consistent variations in mineral chemistry at different $P–T$ conditions, as well as coherent element partitioning; (3) maintenance of constant bulk composition (checked by mass-balance calculations). The use of highly reactive starting materials (gels), combined with the long duration of the experiments, led to the development of coherent textures with mineral phases homogeneously distributed in the charges. Furthermore, the behaviour of seeds can be taken into account to demonstrate a close approach to equilibrium; when not completely absorbed, seeds promoted growth rather than nucleation. As described below, the growth of compositionally homogeneous rims and the occurrence of rather sharp boundaries between non-reacted seeds and newly crystallized phases suggests that the latter approached equilibrium.

RESULTS
Plagioclase-bearing assemblages
Phase assemblages for the two investigated compositions are summarized in Fig. 2. In FLZ, a plagioclase-bearing assemblage composed of olivine, orthopyroxene, clinopyroxene, plagioclase and Cr-spinel is stable up to 0·8 GPa (1100°C) and 0·7 GPa (1000°C). In DLZ, the
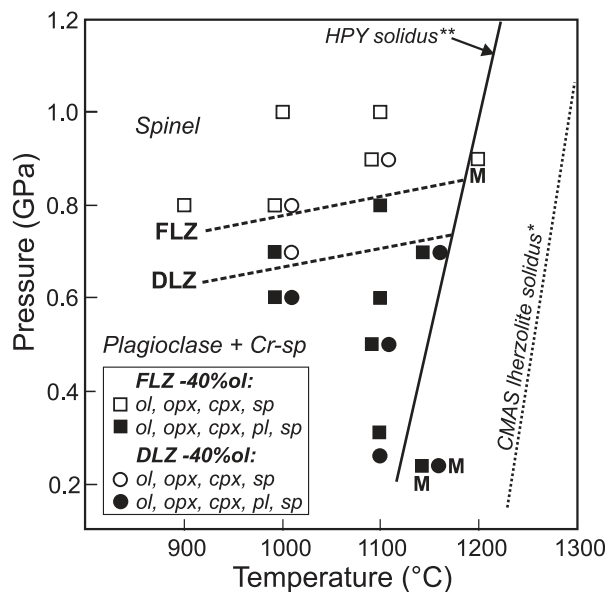

Fig. 2. Phase assemblages in fertile lherzolite FLZ–40% ol (squares) and depleted lherzolite DLZ–40% ol (circles) as a function of pressure and temperature. Also reported are plagioclase-out boundary curves for FLZ and DLZ compositions. 'M' denotes experimental charges containing some glass. The lherzolite solidus in the CMAS system (*) is taken from Presnall *et al.* (1979) and the solidus curve of Hawaiian pyrolite HPY (**) is taken from Jaques & Green (1980).

plagioclase-bearing assemblage was found in experiments up to 0·7 GPa (1150°C) and 0·6 GPa (1000°C). In general, the textural characteristics in experiments on FLZ and DLZ are very similar. Olivine usually occurs as 5–10 μm sized crystals with a rounded habit. Pyroxenes form larger grains (10–30 μm), with euhedral to subhedral habit. Plagioclase is homogeneously distributed in the run charges and is recognizable in BSE images by its dark grey contrast (Fig. 3a and b). It commonly occurs as small, anhedral crystals, ranging from 2 to 15 μm, associated with olivine and interstitial with respect to pyroxenes (Fig. 3a and b). Where anorthite and spinel seeds are not completely reabsorbed, a Na-rich plagioclase rim is observed on the seeds, as confirmed by Na–Ka X-ray mapping. Newly crystallized Cr-bearing spinel grains, not apparently associated with spinel seeds, occur in the plagioclase-bearing assemblage as indicated by Cr–Ka X-ray maps. These newly formed spinels can reach 5–6 μm in size, in high-*T* experiments ($T \geq 1100$°C), allowing reliable compositional analyses.

Plagioclase-free assemblages
In FLZ, a plagioclase-free, spinel-bearing assemblage composed of olivine, orthopyroxene, clinopyroxene and spinel is stable at 0·9 GPa at 1100°C, and 0·8 GPa at 1000°C. In DLZ, the spinel-bearing assemblage appears at lower pressure than FLZ, at 0·7 GPa and 1000°C (Fig. 2). Again, textures in experiments on both FLZ and DLZ are similar. They are characterized by polygonal mineral aggregates and a relatively large grain size (Fig. 3c and d). Olivine forms euhedral to subhedral crystals up to 10 μm in size, often with a rounded habit. Pyroxenes are diffuse and generally occur as elongate prismatic crystals with a regular habit up to 100 μm in length, in higher temperature experiments ($T = 1100$°C). The occurrence of numerous triple points involving both olivine and pyroxenes suggests a well-equilibrated texture (Fig. 3c and d). Spinel is present as small rounded bright crystals up to 5–6 μm in diameter at 1100°C, whereas it forms extremely tiny grains (~1–2 μm) in experiments at 1000°C. In run FLZ1 (1·0 GPa; 1100°C; see Table 2), traces of amphibole (<1 wt % as indicated by mass-balance calculations) were observed as blebs, generally associated with clinopyroxene, indicating slight H_2O contamination in this charge.

Evidence of a quenched melt was recognized based on BSE images at 1150°C, 0·25 GPa and 1200°C, 0·9 GPa in FLZ, and at 1150°C, 0·25 GPa in DLZ. This is suggested by the presence of distinctive textures, in which the minerals form an open, diktytaxitic, network filled with melt blebs up to 7–8 μm in diameter (Fig. 3e and f). Although it is beyond the goal of this study, the $P–T$ conditions of melt occurrence in our experiments have been compared with the solidus reported by Jaques & Green (1980) for Hawaiian pyrolite (HPY), resulting in excellent agreement (see Fig. 2).
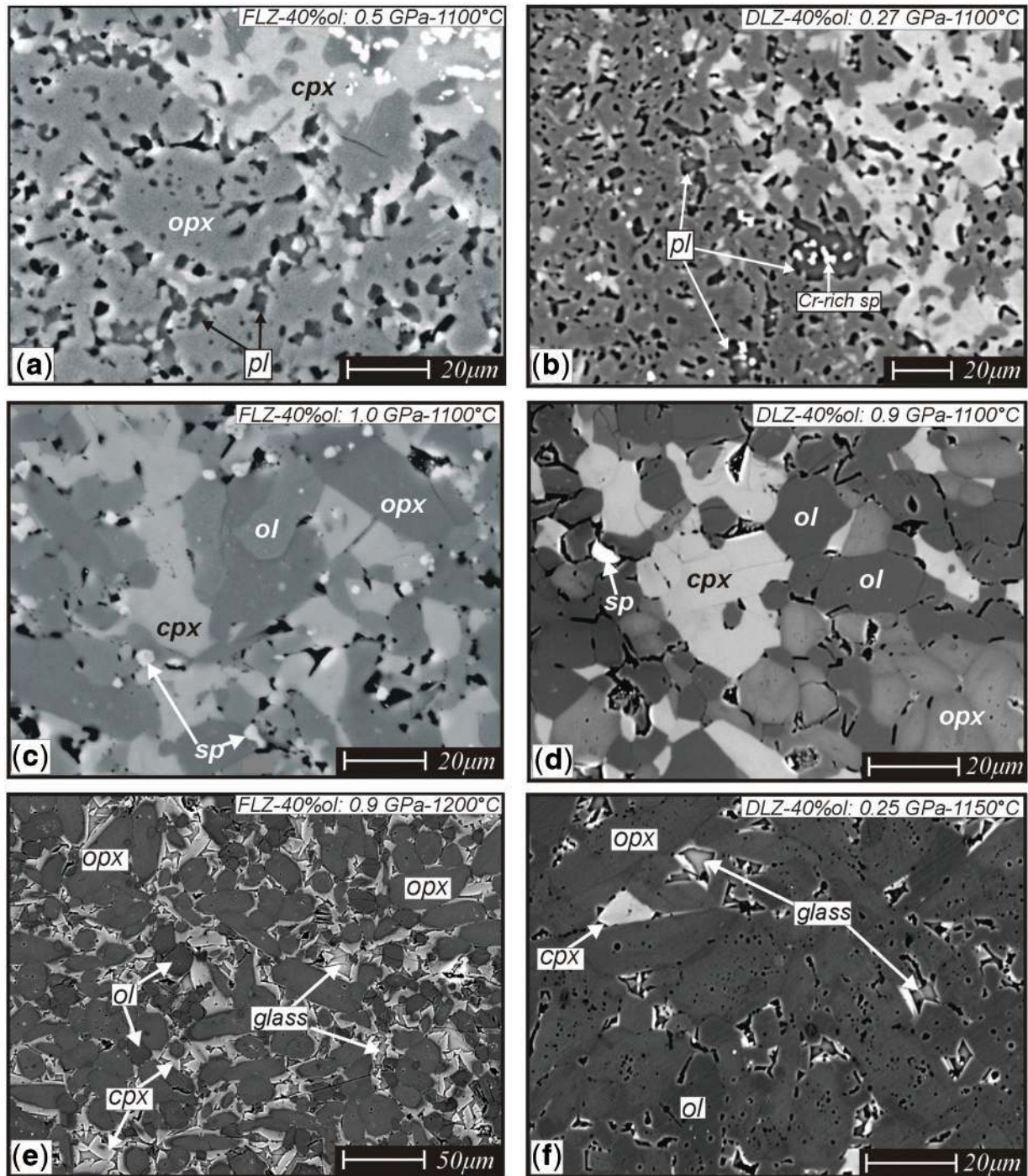
Fig. 3. Representative textures of plagioclase-bearing and plagioclase-free experiments. (a) Back-scattered electron (BSE) image of subsolidus experiment FLZ10 (0·5 GPa; 1100°C): a plagioclase-bearing assemblage is formed of larger grains of orthopyroxene and clinopyroxene and smaller crystals of olivine and plagioclase, the latter occurring as small (up to 5 μm) interstitial grains. (b) BSE image of run DLZ8 (0·27 GPa; 1100°C), exhibiting small Cr-rich spinel grains associated with the plagioclase-bearing assemblage in a depleted lherzolite. (c) BSE image of run FLZ1 (1·0 GPa; 1100°C): spinel-bearing texture with prevailing regular habit of minerals, and spinel occurring in small idiomorphic grains randomly distributed in the mineral matrix. (d) BSE image of run DLZ2 (0·9 GPa; 1100°C), in which the spinel-bearing assemblage is characterized by a coarse polygonal texture. (e) BSE image of run FLZ11 (0·9 GPa; 1200°C): evidence of quenched melt is provided by the presence of diffuse interstitial glass. (f) BSE image of run DLZ9 (0·25 GPa; 1150°C) showing a glass-bearing diktytaxitic texture in depleted lherzolite.

Mineral chemistry

Olivine

The X_{Mg} values [$X_{Mg} = Mg/(Mg + Fe^{tot})$] range from 0·89 to 0·90 in the fertile lherzolite FLZ, and from 0·89 to 0·91 in the depleted lherzolite DLZ, reflecting the bulk composition (Table 3). Olivine composition displays no significant correlation with pressure and temperature. In both FLZ and DLZ, very low TiO_2 contents ($TiO_2 < 0.04$ wt %) were detected in olivine, in agreement with experimental results and thermodynamic calculations proposed by Hermann *et al.* (2005). No Cr was detected in olivine, indicating that chromium in the experimental charges was present predominantly in the trivalent state (Schreiber & Haskin, 1976; Libourel, 1999; Klemme & O'Neill, 2000; Klemme, 2004).

Clinopyroxene

Despite rather uniform X_{Mg} values (0·89–0·91 in FLZ; 0·90–0·91 in DLZ), clinopyroxene displays significant pressure-dependent chemical changes in both bulk compositions (Table 4). In clinopyroxenes from FLZ, the Al content progressively increases with increasing pressure within the plagioclase stability field from 0·149 atoms per formula unit (a.p.f.u.) at 0·31 GPa, 1100°C (FLZ13), to 0·265 a.p.f.u. at 0·8 GPa, 1100°C (FLZ2), up to 0·296 a.p.f.u. at 0·9 GPa, 1100°C (FLZ6) in the spinel lherzolite field (Fig. 4a). Clinopyroxene in DLZ shows a similar progressive Al increase with increasing pressure, although at lower absolute Al concentrations, in agreement with the more depleted bulk composition. In the spinel stability field, Al dependence on pressure is much less pronounced in both compositions because of the different buffering assemblage. A positive correlation with pressure is also shown by the Na content in both FLZ and DLZ. As expected, the jadeite component in clinopyroxene significantly increases across the plagioclase-out boundary as a result of plagioclase breakdown, but also increases with pressure within the plagioclase-facies field. This is well documented by clinopyroxenes in FLZ which are characterized by Na contents varying from 0·021 a.p.f.u. at 0·31 GPa, 1100°C, to 0·081 a.p.f.u. at 1·0 GPa, 1100°C. Cr abundance is rather constant, in the range of 0·017–0·033 a.p.f.u. in FLZ and 0·015–0·033 a.p.f.u. in DLZ. This results in a slight decrease of the X_{Cr} value [$X_{Cr} = Cr/(Cr + Al^{VI})$] with increasing pressure. TiO_2 contents are in the range of 0·10–0·85 wt % in FLZ and 0·06–0·35 wt % in DLZ, with the lowest concentrations in experiments at 1000°C.

Orthopyroxene

Orthopyroxene X_{Mg} values range between 0·89 and 0·90 in both FLZ and DLZ, according to the bulk X_{Mg} values (Tables 1 and 5). The most significant variation is revealed by the Al content, as observed for clinopyroxene.

Al shows a positive correlation with pressure, increasing from 0·117 to 0·229 a.p.f.u. in plagioclase-bearing experiments (from 0·31 to 0·8 GPa), up to 0·237 a.p.f.u. in the plagioclase-free experiments, for the FLZ composition (Fig. 4b). A similar trend at lower Al concentrations is recorded in DLZ orthopyroxenes. Cr contents vary in the range 0·014–0·021 a.p.f.u. in FLZ and 0·015–0·023 a.p.f.u. in DLZ, and are not correlated with pressure or temperature. As described for clinopyroxene, X_{Cr} values [$X_{Cr} = Cr/(Cr + Al^{VI})$] decrease with increasing pressure. Ca contents are low (0·044–0·063 a.p.f.u. in FLZ; 0·038–0·065 a.p.f.u. in DLZ), in agreement with clinopyroxene–orthopyroxene solvus relations at the investigated low T, with some exceptions in run FLZ12 and DLZ14 where the orthopyroxene has relatively high Ca contents, presumably related to intergrowths of clinopyroxene. TiO_2 contents are in the range of 0·05–0·38 wt % in FLZ and 0·03–0·18 wt % in DLZ; as for clinopyroxene, the lowest TiO_2 abundances were found in experiments at 1000°C.

Plagioclase

Despite the small grain size (usually <10 μm) in all of the experiments, reliable plagioclase compositions have been obtained by combining WDS analyses with X-ray element mapping. Plagioclase is characterized by variable anorthite contents [$An = Ca/(Ca + Na)$], which are strikingly correlated with pressure (Table 6). As shown in Fig. 5, An contents in plagioclase progressively decrease with increasing pressure in both bulk compositions. In FLZ at 1100°C, An contents in plagioclase range from 0·82 at 0·31 GPa to 0·59 at 0·8 GPa. Similarly in DLZ, plagioclase An contents range from 0·83 to 0·68 at $P = 0.27–0.7$ GPa. At the same P–T experimental conditions plagioclase displays rather similar An values in the two investigated bulk compositions. This is well documented in experiments at 0·7 GPa and 1150°C, 0·6 GPa and 1000°C, and 0·5 GPa and 1100°C (Fig. 5). Moreover, in the fertile lherzolite FLZ, the slightly lower An contents in plagioclase at 1000°C with respect to plagioclase at 1100–1150°C (as evidenced by runs at 0·6 and 0·7 GPa), could suggest a weak positive correlation with temperature.

Spinel

As described above for plagioclase, combined X-ray mapping and WDS analyses were required for spinels because of their very small grain size (<7 μm) and low modal abundance. Moreover, in cases of very small grain-size textures, spinel compositions had to be derived by removing the effect of the contaminating host minerals (mostly pyroxenes). Unfortunately, in low-T experiments ($T < 1100°C$) extremely fine-grain textures prevented satisfactory chemical analyses. Because oxygen fugacity was not strictly buffered, all iron was considered as Fe^{2+} and Fe^{3+} was not calculated.

Table 3: Representative compositions of olivines

Run:	FLZ1	FLZ6	FLZ2	FLZ12	FLZ7	FLZ5
P (GPa):	1	0·9	0·8	0·8	0·7	0·7
T (°C):	1100	1100	1100	1000	1150	1000
No. An.:	10	10	7	5	8	5
SiO$_2$	40·90 (0·22)	40·70 (0·43)	40·50 (0·21)	40·70 (0·07)	41·00 (0·90)	40·60 (0·15)
TiO$_2$	0·02 (0·04)	0·02 (0·02)	0·06 (0·11)	0·02 (0·01)	0·02 (0·02)	0·04 (0·02)
FeO	10·50 (0·23)	9·69 (0·55)	10·50 (0·32)	10·80 (0·18)	10·60 (0·19)	10·80 (0·24)
MgO	48·60 (0·17)	48·40 (0·90)	48·10 (0·75)	47·50 (0·24)	47·70 (0·76)	47·80 (0·23)
CaO	0·17 (0·08)	0·27 (0·18)	0·23 (0·16)	0·09 (0·03)	0·25 (0·15)	0·11 (0·09)
Total	100·19 (0·25)	99·08 (0·66)	99·39 (0·45)	99·11 (0·14)	99·57 (1·46)	99·35 (0·40)
Si	1·000 (0·006)	1·011 (0·011)	1·000 (0·011)	1·010 (0·002)	1·010 (0·013)	1·010 (0·004)
Ti	0·000 (0·001)	0·000 (0·000)	0·001 (0·002)	0·000 (0·000)	0·000 (0·000)	0·001 (0·000)
Fe	0·215 (0·004)	0·200 (0·013)	0·217 (0·008)	0·223 (0·004)	0·219 (0·004)	0·217 (0·004)
Mg	1·780 (0·004)	1·780 (0·020)	1·770 (0·017)	1·761 (0·008)	1·750 (0·020)	1·750 (0·003)
Ca	0·005 (0·002)	0·007 (0·005)	0·006 (0·004)	0·002 (0·001)	0·007 (0·004)	0·003 (0·002)
Cat· sum	3·000 (0·002)	2·998 (0·003)	2·994 (0·004)	2·996 (0·002)	2·986 (0·004)	2·981 (0·001)
X$_{Mg}$	0·890 (0·003)	0·896 (0·006)	0·888 (0·003)	0·886 (0·002)	0·886 (0·003)	0·887 (0·001)

Run:	FLZ3	FLZ14	FLZ10	FLZ13	DLZ6	DLZ12
P (GPa):	0·6	0·6	0·5	0·31	0·9	0·8
T (°C):	1100	1000	1100	1100	1100	1000
No. An.:	7	4	11	5	13	4
SiO$_2$	40·40 (0·15)	40·60 (0·07)	40·80 (0·36)	41·30 (0·08)	41·20 (0·29)	40·70 (0·08)
TiO$_2$	0·02 (0·02)	0·01 (0·01)	0·02 (0·02)	0·02 (0·02)	0·01 (0·02)	0·03 (0·01)
FeO	10·80 (0·18)	10·50 (0·09)	10·70 (0·28)	10·60 (0·18)	7·98 (0·45)	8·34 (0·03)
MgO	48·00 (1·01)	49·00 (0·18)	47·90 (0·65)	47·30 (0·43)	49·70 (0·80)	49·40 (0·13)
CaO	0·22 (0·03)	0·10 (0·09)	0·30 (0·21)	0·61 (0·39)	0·22 (0·13)	0·16 (0·04)
Total	99·45 (0·74)	100·21 (0·13)	99·72 (0·60)	99·90 (0·36)	99·12 (0·50)	98·62 (0·08)
Si	0·997 (0·011)	0·993 (0·003)	1·000 (0·011)	1·020 (0·002)	1·010 (0·005)	1·000 (0·004)
Ti	0·000 (0·000)	0·000 (0·000)	0·000 (0·000)	0·000 (0·000)	0·000 (0·000)	0·001 (0·000)
Fe	0·222 (0·006)	0·215 (0·002)	0·220 (0·006)	0·219 (0·003)	0·162 (0·010)	0·172 (0·001)
Mg	1·760 (0·019)	1·790 (0·005)	1·760 (0·014)	1·740 (0·008)	1·820 (0·018)	1·820 (0·002)
Ca	0·006 (0·001)	0·003 (0·002)	0·008 (0·005)	0·016 (0·010)	0·006 (0·004)	0·004 (0·001)
Cat· sum	2·985 (0·002)	3·001 (0·002)	2·988 (0·003)	2·995 (0·004)	2·998 (0·003)	2·997 (0·001)
X$_{Mg}$	0·885 (0·003)	0·891 (0·002)	0·885 (0·004)	0·881 (0·004)	0·914 (0·006)	0·912 (0·001)

Run:	DLZ7	DLZ5	DLZ14	DLZ10	DLZ8
P (GPa):	0·7	0·7	0·6	0·5	0·27
T (°C):	1150	1000	1000	1100	1100
No. An.:	7	6	5	8	6
SiO$_2$	41·10 (0·19)	41·20 (0·17)	40·80 (0·11)	40·70 (0·33)	41·20 (0·84)
TiO$_2$	0·02 (0·02)	0·01 (0·02)	0·00 (0·01)	0·02 (0·02)	0·02 (0·02)
FeO	10·60 (0·20)	10·50 (0·18)	10·10 (0·06)	10·70 (0·32)	9·40 (0·17)
MgO	47·50 (0·24)	47·50 (0·26)	49·00 (0·14)	48·10 (0·64)	49·50 (0·24)
CaO	0·22 (0·15)	0·22 (0·16)	0·15 (0·05)	0·28 (0·08)	0·16 (0·07)
Total	99·44 (0·30)	99·44 (0·32)	100·05 (0·07)	99·80 (0·45)	100·28 (0·52)
Si	1·020 (0·005)	1·020 (0·005)	0·998 (0·002)	0·999 (0·013)	1·000 (0·017)
Ti	0·000 (0·000)	0·000 (0·000)	0·000 (0·000)	0·000 (0·000)	0·000 (0·000)
Fe	0·219 (0·004)	0·218 (0·004)	0·206 (0·001)	0·220 (0·005)	0·191 (0·004)
Mg	1·750 (0·009)	1·750 (0·009)	1·790 (0·004)	1·760 (0·015)	1·800 (0·014)
Ca	0·006 (0·004)	0·006 (0·004)	0·004 (0·001)	0·007 (0·002)	0·004 (0·002)
Cat·sum	2·995 (0·002)	2·994 (0·004)	2·998 (0·001)	2·987 (0·004)	2·996 (0·005)
X$_{Mg}$	0·886 (0·004)	0·887 (0·004)	0·895 (0·001)	0·886 (0·002)	0·902 (0·001)

$X_{Mg} = Mg/(Mg + Fe^{tot})$. Numbers in parentheses correspond to 1σ standard deviations. Cations are calculated on the basis of 4 oxygens and all $Fe = Fe^{2+}$.

Table 4: Representative compositions of clinopyroxenes

Run:	FLZ1	FLZ6	FLZ2	FLZ12	FLZ7	FLZ5	FLZ3
P (GPa):	1	0·9	0·8	0·8	0·7	0·7	0·6
T (°C):	1100	1100	1100	1000	1150	1000	1100
No. An.:	21	13	11	8	13	6	8
SiO_2	52·50 (0·52)	51·10 (0·33)	51·80 (0·48)	52·60 (0·44)	51·80 (0·71)	51·60 (0·43)	52·10 (0·71)
TiO_2	0·32 (0·06)	0·85 (0·22)	0·39 (0·15)	0·10 (0·04)	0·39 (0·20)	0·10 (0·04)	0·41 (0·20)
Al_2O_3	6·85 (0·27)	6·92 (0·34)	6·24 (0·57)	5·71 (0·16)	5·48 (0·52)	5·47 (0·19)	4·87 (0·17)
Cr_2O_3	0·77 (0·13)	0·86 (0·10)	0·78 (0·18)	0·58 (0·07)	0·83 (0·09)	0·59 (0·19)	0·83 (0·14)
FeO	3·45 (0·15)	3·21 (0·14)	3·47 (0·22)	3·29 (0·17)	3·45 (0·22)	3·08 (0·31)	3·50 (0·17)
MgO	16·60 (0·46)	16·60 (0·55)	17·20 (0·39)	16·80 (0·28)	17·20 (0·87)	17·60 (0·64)	17·60 (0·61)
CaO	18·90 (0·42)	19·00 (0·27)	19·30 (0·81)	20·20 (0·44)	19·90 (0·77)	20·30 (0·94)	19·80 (0·47)
Na_2O	1·16 (0·17)	0·92 (0·06)	0·75 (0·09)	0·91 (0·08)	0·47 (0·06)	0·42 (0·10)	0·47 (0·10)
Total	100·54 (0·59)	99·45 (0·50)	99·94 (0·98)	100·19 (0·35)	99·52 (0·82)	99·16 (0·50)	99·58 (0·35)
Si	1·881 (0·013)	1·853 (0·008)	1·872 (0·011)	1·896 (0·009)	1·882 (0·013)	1·879 (0·009)	1·891 (0·022)
Ti	0·009 (0·002)	0·023 (0·006)	0·011 (0·004)	0·003 (0·001)	0·011 (0·005)	0·003 (0·001)	0·011 (0·005)
Al(IV)	0·119 (0·013)	0·147 (0·008)	0·128 (0·011)	0·104 (0·010)	0·118 (0·013)	0·121 (0·009)	0·109 (0·022)
Al(VI)	0·170 (0·007)	0·149 (0·012)	0·137 (0·022)	0·138 (0·005)	0·116 (0·016)	0·114 (0·016)	0·100 (0·015)
Cr	0·022 (0·004)	0·025 (0·003)	0·022 (0·005)	0·017 (0·002)	0·024 (0·002)	0·017 (0·005)	0·024 (0·004)
Fe	0·104 (0·004)	0·098 (0·004)	0·105 (0·006)	0·099 (0·005)	0·105 (0·006)	0·094 (0·009)	0·106 (0·005)
Mg	0·886 (0·025)	0·897 (0·026)	0·925 (0·024)	0·903 (0·011)	0·933 (0·045)	0·957 (0·032)	0·955 (0·034)
Ca	0·725 (0·016)	0·739 (0·011)	0·747 (0·030)	0·781 (0·020)	0·774 (0·033)	0·792 (0·040)	0·770 (0·017)
Na	0·081 (0·012)	0·064 (0·004)	0·053 (0·006)	0·064 (0·005)	0·033 (0·004)	0·030 (0·007)	0·033 (0·007)
Cat. sum	3·996 (0·008)	3·995 (0·009)	4·000 (0·008)	4·004 (0·005)	3·995 (0·010)	4·006 (0·010)	3·999 (0·015)
X_{Mg}	0·895 (0·004)	0·902 (0·005)	0·898 (0·005)	0·901 (0·006)	0·899 (0·004)	0·911 (0·007)	0·900 (0·005)

Run:	FLZ14	FLZ10	FLZ13	DLZ6	DLZ12	DLZ7	DLZ5
P (GPa):	0·6	0·5	0·31	0·9	0·8	0·7	0·7
T (°C):	1000	1100	1100	1100	1000	1150	1000
No. An.:	9	11	9	8	5	10	6
SiO_2	52·50 (0·38)	51·90 (0·39)	53·10 (0·88)	51·60 (0·30)	52·80 (0·20)	51·60 (0·78)	50·40 (0·74)
TiO_2	0·15 (0·05)	0·55 (0·22)	0·24 (0·03)	0·35 (0·02)	0·12 (0·04)	0·25 (0·11)	0·06 (0·00)
Al_2O_3	5·16 (0·35)	4·58 (0·27)	3·49 (0·30)	5·60 (0·56)	5·11 (0·11)	5·36 (0·91)	5·57 (0·81)
Cr_2O_3	0·63 (0·10)	1·15 (0·10)	0·89 (0·41)	1·02 (0·12)	0·61 (0·05)	0·82 (0·16)	0·69 (0·03)
FeO	3·30 (0·18)	3·57 (0·27)	3·70 (0·22)	3·13 (0·16)	2·80 (0·10)	3·24 (0·29)	2·26 (0·27)
MgO	17·30 (0·90)	17·80 (0·71)	18·60 (0·56)	17·50 (0·22)	17·30 (0·05)	17·20 (0·87)	15·50 (0·29)
CaO	21·30 (1·24)	19·60 (0·61)	19·60 (0·43)	19·70 (0·27)	21·50 (0·19)	19·90 (1·05)	23·70 (0·33)
Na_2O	0·43 (0·05)	0·42 (0·03)	0·29 (0·07)	0·81 (0·04)	0·79 (0·07)	0·57 (0·12)	0·15 (0·05)
Total	100·78 (0·28)	99·57 (0·40)	99·92 (0·85)	99·71 (0·31)	101·02 (0·08)	98·95 (0·72)	98·33 (0·26)
Si	1·888 (0·013)	1·888 (0·010)	1·920 (0·011)	1·875 (0·015)	1·895 (0·006)	1·884 (0·020)	1·866 (0·021)
Ti	0·004 (0·001)	0·015 (0·006)	0·007 (0·001)	0·010 (0·000)	0·003 (0·001)	0·007 (0·003)	0·002 (0·000)
Al(IV)	0·112 (0·013)	0·112 (0·009)	0·080 (0·011)	0·125 (0·015)	0·105 (0·006)	0·116 (0·019)	0·134 (0·021)
Al(VI)	0·107 (0·018)	0·085 (0·008)	0·069 (0·005)	0·114 (0·012)	0·111 (0·002)	0·115 (0·024)	0·110 (0·016)
Cr	0·018 (0·003)	0·033 (0·003)	0·025 (0·011)	0·029 (0·003)	0·017 (0·001)	0·024 (0·005)	0·020 (0·001)
Fe	0·099 (0·006)	0·108 (0·008)	0·112 (0·008)	0·095 (0·005)	0·084 (0·003)	0·099 (0·009)	0·070 (0·009)
Mg	0·926 (0·048)	0·963 (0·035)	1·000 (0·019)	0·949 (0·011)	0·927 (0·002)	0·938 (0·047)	0·854 (0·013)
Ca	0·821 (0·048)	0·763 (0·026)	0·759 (0·025)	0·765 (0·012)	0·825 (0·008)	0·778 (0·039)	0·939 (0·009)
Na	0·030 (0·003)	0·030 (0·002)	0·021 (0·005)	0·058 (0·003)	0·057 (0·005)	0·041 (0·009)	0·011 (0·004)
Cat. sum	4·005 (0·012)	3·996 (0·008)	3·993 (0·013)	4·020 (0·008)	4·024 (0·006)	4·001 (0·008)	4·006 (0·005)
X_{Mg}	0·903 (0·006)	0·899 (0·005)	0·900 (0·008)	0·909 (0·004)	0·917 (0·003)	0·905 (0·004)	0·924 (0·010)

Table 4: Continued

Run:	DLZ14	DLZ10	DLZ8
P (GPa):	0·6	0·5	0·27
T (°C):	1000	1100	1100
No. An.:	7	9	14
SiO$_2$	52·20 (0·28)	52·10 (0·31)	53·60 (0·76)
TiO$_2$	0·14 (0·03)	0·22 (0·07)	0·26 (0·06)
Al$_2$O$_3$	4·12 (0·11)	4·30 (0·10)	3·04 (0·45)
Cr$_2$O$_3$	0·53 (0·06)	0·96 (0·04)	1·14 (0·16)
FeO	3·16 (0·09)	3·37 (0·21)	3·02 (0·28)
MgO	17·70 (0·42)	18·00 (0·36)	19·20 (0·59)
CaO	21·90 (0·14)	20·20 (0·36)	19·60 (0·79)
Na$_2$O	0·28 (0·04)	0·41 (0·05)	0·24 (0·10)
Total	100·03 (0·23)	99·56 (0·31)	100·10 (0·82)
Si	1·895 (0·009)	1·895 (0·010)	1·929 (0·016)
Ti	0·004 (0·001)	0·006 (0·002)	0·007 (0·002)
Al(IV)	0·105 (0·009)	0·105 (0·010)	0·071 (0·016)
Al(VI)	0·072 (0·007)	0·079 (0·009)	0·058 (0·012)
Cr	0·015 (0·002)	0·028 (0·001)	0·033 (0·005)
Fe	0·096 (0·003)	0·103 (0·007)	0·091 (0·009)
Mg	0·957 (0·022)	0·978 (0·020)	1·030 (0·037)
Ca	0·852 (0·006)	0·786 (0·013)	0·758 (0·027)
Na	0·020 (0·003)	0·029 (0·003)	0·017 (0·007)
Cat. sum	4·015 (0·007)	4·009 (0·009)	3·993 (0·013)
X_{Mg}	0·909 (0·004)	0·905 (0·004)	0·919 (0·007)

$X_{Mg} = Mg/(Mg + Fe^{tot})$. Numbers in parentheses correspond to 1σ standard deviations. Cations are calculated on the basis of 6 oxygens and all $Fe = Fe^{2+}$.

Spinel exhibits marked compositional variations as a function of pressure (Table 7). X_{Mg} increases with pressure ($X_{Mg} = 0\cdot72–0\cdot82$ in FLZ; $X_{Mg} = 0\cdot76–0\cdot82$ in DLZ), whereas X_{Cr} [$X_{Cr} = Cr/(Cr + Al)$] is inversely correlated with *P* in both bulk compositions (Fig. 6a). In FLZ, X_{Cr} values progressively decrease from 0·29 at 0·31 GPa to 0·08 at 1·0 GPa in the spinel-facies field (Fig. 6a and b). Relatively higher X_{Cr} values were observed in spinels from DLZ, in agreement with the higher bulk Cm/An ratio (see Fig. 6 and Table 1). An analogous behaviour is shown by the TiO$_2$ content, resulting in a positive TiO$_2$–X_{Cr} correlation (Fig. 6b). The highest TiO$_2$ contents were found in spinels at low pressure, in the fertile lherzolite at 0·5 GPa (TiO$_2$ = 0·76 wt %) and in the depleted lherzolite at 0·27 GPa (TiO$_2$ = 0·40 wt %).

DISCUSSION
Element partitioning
X_{Mg} values for olivine, orthopyroxene and clinopyroxene are not sensitive to temperature and pressure. Previous experimental studies have indicated that near 1000°C the Fe/Mg ratio does not affect sensitively the high-pressure stability limit of the plagioclase-facies assemblage, but rather it influences the nature of the reaction products; at intermediate values, this involves the appearance of Fe-rich garnet together with spinel (e.g. Kushiro & Yoder, 1966; Green & Hibberson, 1970). However, at bulk-rock X_{Mg} values comparable with ultramafic compositions the effect of Fe on the pressure stability of plagioclase is
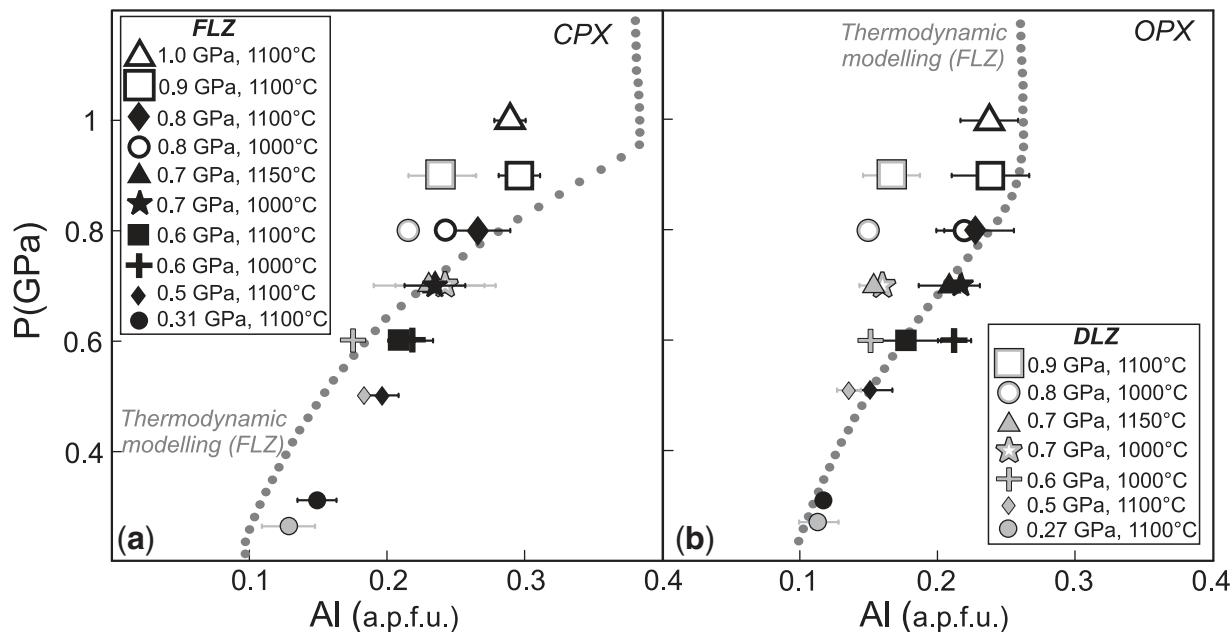

Fig. 4. Al content (Al^{IV} + Al^{VI} a.p.f.u. in Tables 4 and 5) variations in clinopyroxene (a) and orthopyroxene (b) from experiments on FLZ (black symbols) and DLZ (grey symbols) as a function of pressure. Filled symbols correspond to plagioclase-bearing experiments; open symbols indicate plagioclase-free experiments. The grey dotted curve corresponds to the Al variation trend in pyroxenes, calculated at $T = 1100$°C for the FLZ composition using Perple_X software (Connolly, 1990; Connolly & Petrini, 2002).

Table 5: Representative compositions of orthopyroxenes

Run:	FLZ1	FLZ6	FLZ2	FLZ12	FLZ7	FLZ5	FLZ3
P (GPa):	1	0·9	0·8	0·8	0·7	0·7	0·6
T (°C):	1100	1100	1100	1000	1150	1000	1100
No. An.:	16	20	13	8	12	7	11
SiO_2	54·40 (0·61)	53·70 (0·56)	53·90 (0·62)	54·20 (0·28)	54·60 (0·40)	54·10 (0·21)	55·20 (0·56)
TiO_2	0·11 (0·07)	0·32 (0·11)	0·23 (0·13)	0·11 (0·10)	0·29 (0·07)	0·05 (0·02)	0·13 (0·04)
Al_2O_3	5·84 (0·53)	5·81 (0·69)	5·54 (0·68)	5·39 (0·36)	5·10 (0·57)	5·29 (0·11)	4·33 (0·63)
Cr_2O_3	0·57 (0·06)	0·60 (0·07)	0·69 (0·06)	0·54 (0·13)	0·68 (0·09)	0·60 (0·03)	0·71 (0·06)
FeO	6·69 (0·14)	6·23 (0·26)	6·50 (0·21)	6·59 (0·27)	6·58 (0·12)	6·50 (0·25)	6·50 (0·36)
MgO	31·50 (0·57)	31·40 (0·59)	31·30 (0·51)	32·20 (0·16)	31·20 (0·34)	32·00 (0·29)	31·70 (0·14)
CaO	1·39 (0·16)	1·57 (0·15)	1·64 (0·15)	1·45 (0·28)	1·61 (0·16)	1·17 (0·16)	1·50 (0·18)
Na_2O	0·09 (0·06)	0·06 (0·05)	0·05 (0·05)	0·12 (0·03)	0·06 (0·01)	0·09 (0·04)	0·06 (0·02)
Total	100·58 (0·35)	99·69 (0·37)	99·85 (0·45)	100·60 (0·33)	100·12 (0·79)	99·80 (0·32)	100·13 (0·47)
Si	1·875 (0·020)	1·867 (0·021)	1·873 (0·020)	1·869 (0·007)	1·890 (0·012)	1·878 (0·006)	1·910 (0·014)
Ti	0·003 (0·002)	0·008 (0·003)	0·006 (0·003)	0·003 (0·003)	0·007 (0·002)	0·001 (0·000)	0·003 (0·001)
Al(IV)	0·125 (0·020)	0·133 (0·021)	0·127 (0·020)	0·131 (0·007)	0·110 (0·012)	0·122 (0·006)	0·090 (0·014)
Al(VI)	0·112 (0·017)	0·105 (0·015)	0·100 (0·018)	0·088 (0·008)	0·098 (0·011)	0·095 (0·008)	0·087 (0·015)
Cr	0·015 (0·002)	0·017 (0·002)	0·019 (0·002)	0·015 (0·003)	0·019 (0·003)	0·016 (0·001)	0·019 (0·002)
Fe	0·193 (0·004)	0·181 (0·008)	0·189 (0·006)	0·190 (0·008)	0·191 (0·005)	0·189 (0·007)	0·188 (0·011)
Mg	1·620 (0·031)	1·630 (0·026)	1·620 (0·022)	1·660 (0·005)	1·610 (0·011)	1·660 (0·013)	1·630 (0·011)
Ca	0·051 (0·006)	0·058 (0·006)	0·061 (0·006)	0·054 (0·010)	0·060 (0·006)	0·044 (0·006)	0·056 (0·007)
Na	0·006 (0·004)	0·004 (0·003)	0·004 (0·003)	0·008 (0·002)	0·004 (0·001)	0·006 (0·003)	0·004 (0·001)
Cat. sum	4·000 (0·013)	4·003 (0·010)	3·999 (0·008)	4·017 (0·002)	3·989 (0·003)	4·011 (0·007)	3·987 (0·006)
X_{Mg}	0·894 (0·004)	0·900 (0·005)	0·896 (0·004)	0·897 (0·004)	0·894 (0·003)	0·898 (0·003)	0·897 (0·005)

Run:	FLZ14	FLZ10	FLZ13	DLZ6	DLZ12	DLZ7	DLZ5
P (GPa):	0·6	0·5	0·31	0·9	0·8	0·7	0·7
T (°C):	1000	1100	1100	1100	1000	1150	1000
No. An.:	8	8	9	12	6	14	7
SiO_2	54·10 (0·24)	55·00 (0·43)	55·50 (0·09)	54·90 (0·49)	55·20 (0·31)	54·90 (0·53)	54·60 (0·31)
TiO_2	0·11 (0·08)	0·38 (0·05)	0·28 (0·07)	0·13 (0·01)	0·03 (0·01)	0·12 (0·07)	0·11 (0·01)
Al_2O_3	5·18 (0·30)	3·67 (0·39)	2·84 (0·13)	4·06 (0·50)	3·66 (0·15)	3·72 (0·24)	3·91 (0·15)
Cr_2O_3	0·66 (0·07)	0·75 (0·07)	0·52 (0·06)	0·72 (0·10)	0·56 (0·03)	0·62 (0·05)	0·70 (0·03)
FeO	6·42 (0·28)	6·61 (0·22)	6·50 (0·06)	6·35 (0·26)	6·62 (0·11)	6·58 (0·19)	6·83 (0·11)
MgO	32·10 (0·61)	31·70 (0·29)	31·90 (0·18)	31·70 (0·66)	32·60 (0·10)	31·60 (0·39)	32·14 (0·10)
CaO	1·30 (0·36)	1·64 (0·09)	1·69 (0·06)	1·67 (0·20)	1·14 (0·05)	1·52 (0·20)	1·01 (0·05)
Na_2O	0·05 (0·03)	0·05 (0·02)	0·07 (0·02)	0·06 (0·02)	0·04 (0·01)	0·05 (0·01)	0·00 (0·01)
Total	99·92 (0·13)	99·80 (0·32)	99·30 (0·22)	99·59 (0·37)	99·85 (0·05)	99·12 (0·62)	99·30 (0·05)
Si	1·878 (0·007)	1·913 (0·016)	1·937 (0·001)	1·910 (0·015)	1·914 (0·009)	1·920 (0·011)	1·900 (0·009)
Ti	0·003 (0·002)	0·010 (0·002)	0·007 (0·002)	0·003 (0·000)	0·001 (0·000)	0·003 (0·002)	0·003 (0·000)
Al(IV)	0·122 (0·007)	0·087 (0·016)	0·063 (0·001)	0·090 (0·015)	0·086 (0·009)	0·080 (0·011)	0·100 (0·014)
Al(VI)	0·090 (0·017)	0·064 (0·008)	0·054 (0·004)	0·077 (0·011)	0·064 (0·003)	0·074 (0·008)	0·061 (0·015)
Cr	0·018 (0·002)	0·021 (0·002)	0·014 (0·002)	0·020 (0·003)	0·015 (0·001)	0·017 (0·001)	0·019 (0·001)
Fe	0·186 (0·008)	0·192 (0·006)	0·190 (0·001)	0·185 (0·007)	0·192 (0·003)	0·193 (0·005)	0·199 (0·003)
Mg	1·660 (0·032)	1·640 (0·013)	1·660 (0·012)	1·640 (0·032)	1·690 (0·006)	1·650 (0·017)	1·690 (0·006)
Ca	0·048 (0·013)	0·061 (0·003)	0·063 (0·002)	0·062 (0·007)	0·043 (0·002)	0·057 (0·007)	0·038 (0·002)
Na	0·004 (0·002)	0·004 (0·001)	0·005 (0·001)	0·004 (0·001)	0·003 (0·001)	0·004 (0·001)	0·000 (0·001)
Cat. sum	4·008 (0·011)	3·991 (0·008)	3·993 (0·004)	3·991 (0·008)	4·007 (0·006)	3·998 (0·008)	4·010 (0·006)
X_{Mg}	0·899 (0·003)	0·895 (0·003)	0·897 (0·001)	0·899 (0·005)	0·898 (0·001)	0·895 (0·003)	0·895 (0·001)

Table 5: Continued

Run:	DLZ14	DLZ10	DLZ8
P (GPa):	0·6	0·5	0·27
T (°C):	1000	1100	1100
No. An.:	5	13	11
SiO$_2$	54·70 (0·09)	55·20 (0·25)	55·90 (0·57)
TiO$_2$	0·05 (0·02)	0·13 (0·05)	0·18 (0·03)
Al$_2$O$_3$	3·69 (0·07)	3·31 (0·22)	2·81 (0·36)
Cr$_2$O$_3$	0·58 (0·03)	0·66 (0·03)	0·85 (0·12)
FeO	6·40 (0·09)	6·66 (0·15)	6·23 (0·20)
MgO	32·60 (0·28)	32·00 (0·28)	33·10 (0·60)
CaO	1·48 (0·16)	1·64 (0·15)	1·77 (0·08)
Na$_2$O	0·02 (0·01)	0·06 (0·02)	0·04 (0·02)
Total	99·53 (0·44)	99·66 (0·48)	100·88 (0·22)
Si	1·906 (0·006)	1·923 (0·011)	1·921 (0·013)
Ti	0·001 (0·001)	0·004 (0·001)	0·005 (0·001)
Al(IV)	0·094 (0·006)	0·077 (0·011)	0·079 (0·013)
Al(VI)	0·058 (0·005)	0·059 (0·007)	0·035 (0·021)
Cr	0·016 (0·001)	0·018 (0·001)	0·023 (0·003)
Fe	0·186 (0·002)	0·194 (0·004)	0·179 (0·007)
Mg	1·690 (0·009)	1·660 (0·011)	1·700 (0·035)
Ca	0·055 (0·006)	0·061 (0·005)	0·065 (0·003)
Na	0·002 (0·001)	0·004 (0·002)	0·003 (0·001)
Cat. sum	4·007 (0·006)	3·999 (0·009)	4·010 (0·017)
X_{Mg}	0·901 (0·001)	0·895 (0·002)	0·904 (0·002)

$X_{Mg} = Mg/(Mg + Fe^{tot})$. Numbers in parentheses correspond to 1σ standard deviations. Cations are calculated on the basis of 6 oxygens and all Fe = Fe^{2+}.

expected to be small (Green & Hibberson, 1970; Green & Falloon, 1998).

Within the limited range of *P*–*T* conditions investigated in this study, olivine, orthopyroxene and clinopyroxene preferentially partition Mg relative to spinel, in agreement with previous experimental studies on comparable ultramafic compositions at different *P*–*T* conditions (Falloon *et al.*, 1997, 1999; Niida & Green, 1999; Fumagalli & Poli, 2005). The Fe–Mg partitioning thus allows assessment of the achievement of equilibrium in experimental charges.

Alkalis and Cr–Al partitioning instead show significant variations as a function of pressure, and are useful for the quantification of the continuous reaction controlling the transition between plagioclase lherzolite and spinel lherzolite.

Ca–Na partitioning

In mantle peridotites at plagioclase-stability conditions, Ca and Na are mostly partitioned between plagioclase and clinopyroxene. In terms of solid solutions, the Ca–Na partitioning between plagioclase and clinopyroxene is controlled by the exchange reaction

$$\underset{\text{clinopyroxene}}{NaAlSi_2O_6} + \underset{\text{plagioclase}}{CaAl_2Si_2O_8} = \underset{\text{clinopyroxene}}{CaAl_2SiO_6} + \underset{\text{plagioclase}}{NaAlSi_3O_8}. \quad (4)$$
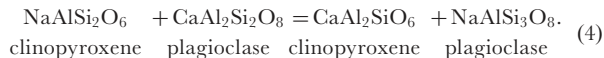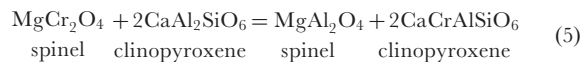
Ca/(Ca + Na) ratios in plagioclase and clinopyroxene are positively correlated and decrease with increasing pressure (Fig. 7). This implies that near the plagioclase-out boundary an albite-rich plagioclase is associated with a relatively Na-rich clinopyroxene. A minor influence of temperature on Ca–Na partitioning is suggested by the slight shift towards lower An contents in plagioclase from experiments performed at 1000°C, relative to experiments at 1100°C (see Fig. 5).
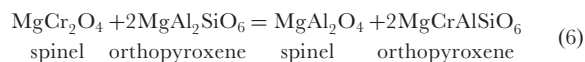
The results for FLZ and DLZ are consistent with the experimental data of (1) Falloon *et al.* (1997), for a single subsolidus experiment at 1·0 GPa and 1250°C on MM3 lherzolite in a complex system, and (2) Niida & Green (1999) on 'MORB' pyrolite in an hydrous complex system (at 0·5 GPa and 925°C). In Niida & Green's experiments the occurrence of high modal amounts of pargasitic amphibole (26·5 wt %) coexisting with plagioclase shifts the An content of the plagioclase and the Ca/(Ca + Na) of clinopyroxene toward higher values (Fig. 7).
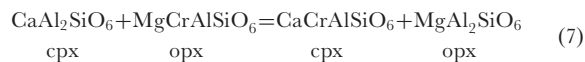
Cr–Al partitioning

Cr and Al are hosted in spinel, orthopyroxene and clinopyroxene through the end-members Mg-chromite (MgCr$_2$O$_4$), Mg,Cr-Tschermak (2MgCrAlSiO$_6$ = MgAl$_2$SiO$_6$ + MgCr$_2$SiO$_6$) and Ca,Cr-Tschermak (2CaCrAlSiO$_6$ = CaAl$_2$SiO$_6$ + CaCr$_2$SiO$_6$). The Cr–Al partitioning between spinel and pyroxenes is governed by the exchange reactions

$$\underset{\text{spinel}}{MgCr_2O_4} + \underset{\text{clinopyroxene}}{2CaAl_2SiO_6} = \underset{\text{spinel}}{MgAl_2O_4} + \underset{\text{clinopyroxene}}{2CaCrAlSiO_6} \quad (5)$$

and

$$\underset{\text{spinel}}{MgCr_2O_4} + \underset{\text{orthopyroxene}}{2MgAl_2SiO_6} = \underset{\text{spinel}}{MgAl_2O_4} + \underset{\text{orthopyroxene}}{2MgCrAlSiO_6} \quad (6)$$

and the Cr–Al partitioning between clino- and orthopyroxene is controlled by the reaction

$$\underset{\text{cpx}}{CaAl_2SiO_6} + \underset{\text{opx}}{MgCrAlSiO_6} = \underset{\text{cpx}}{CaCrAlSiO_6} + \underset{\text{opx}}{MgAl_2SiO_6} \quad (7)$$

In both FLZ and DLZ compositions the X_{Cr} of spinel is positively correlated with X_{Cr} of both clinopyroxene and orthopyroxene; the marked X_{Cr} decrease in spinel is coupled with a slight and systematic X_{Cr} decrease in pyroxenes with increasing pressure (Fig. 8). This indicates, as expected, that spinel changes from a chrome-rich to an aluminous spinel through the transition and that, within the multivariant plagioclase-bearing field, although spinel preferentially incorporates Cr, pyroxenes are also important hosts of Cr in peridotitic systems (Webb & Wood, 1986; Klemme & O'Neill, 2000). It is noteworthy that

Table 6: Representative compositions of plagioclases

Sample:	FLZ2	FLZ7	FLZ5	FLZ3	FLZ14	FLZ10
P (GPa):	0·8	0·7	0·7	0·6	0·6	0·5
T (°C):	1100	1150	1000	1100	1000	1100
No. An.:	11	11	6	12	6	15
SiO_2	53·80 (0·96)	51·40 (0·59)	53·60 (0·36)	52·60 (0·72)	51·60 (0·50)	50·00 (1·26)
TiO_2	0·03 (0·03)	0·02 (0·02)	0·07 (0·04)	0·07 (0·05)	0·05 (0·04)	0·06 (0·04)
Al_2O_3	29·00 (1·14)	29·50 (0·84)	29·30 (0·42)	29·80 (0·71)	29·90 (0·14)	31·70 (1·00)
Cr_2O_3	0·11 (0·05)	0·04 (0·06)	0·10 (0·05)	0·07 (0·05)	0·07 (0·04)	0·10 (0·11)
FeO	0·05 (0·15)	0·23 (0·19)	0·03 (0·04)	0·09 (0·13)	0·09 (0·05)	0·16 (0·27)
MgO	0·02 (0·04)	0·38 (0·31)	0·02 (0·02)	0·09 (0·19)	0·10 (0·07)	0·39 (0·61)
CaO	12·20 (0·71)	13·60 (0·92)	13·00 (0·04)	13·90 (0·78)	14·20 (0·49)	15·10 (0·48)
Na_2O	4·68 (0·31)	3·63 (0·30)	4·34 (0·07)	3·50 (0·27)	3·94 (0·16)	2·71 (0·27)
Total	99·88 (0·96)	98·80 (0·75)	100·46 (0·04)	100·11 (0·91)	99·95 (0·16)	100·23 (0·54)
Si	2·440 (0·046)	2·370 (0·036)	2·420 (0·018)	2·400 (0·033)	2·350 (0·025)	2·280 (0·061)
Ti	0·001 (0·001)	0·001 (0·001)	0·002 (0·001)	0·002 (0·002)	0·002 (0·001)	0·002 (0·001)
Al	1·550 (0·055)	1·600 (0·038)	1·560 (0·021)	1·600 (0·033)	1·600 (0·008)	1·700 (0·050)
Cr	0·004 (0·002)	0·001 (0·002)	0·004 (0·002)	0·002 (0·002)	0·002 (0·001)	0·004 (0·004)
Fe	0·002 (0·006)	0·009 (0·007)	0·001 (0·001)	0·003 (0·005)	0·003 (0·002)	0·006 (0·009)
Mg	0·002 (0·003)	0·026 (0·021)	0·001 (0·001)	0·006 (0·013)	0·007 (0·005)	0·027 (0·041)
Ca	0·594 (0·034)	0·671 (0·042)	0·627 (0·002)	0·680 (0·035)	0·690 (0·023)	0·739 (0·023)
Na	0·411 (0·024)	0·324 (0·027)	0·380 (0·006)	0·309 (0·025)	0·347 (0·014)	0·239 (0·024)
Cat·sum	5·003 (0·016)	5·002 (0·013)	4·995 (0·006)	5·003 (0·016)	5·001 (0·012)	4·996 (0·028)
(Na+Ca)	1·005 (0·029)	0·995 (0·028)	1·007 (0·005)	0·989 (0·021)	1·037 (0·018)	0·978 (0·029)
An	0·591 (0·025)	0·674 (0·030)	0·623 (0·004)	0·687 (0·027)	0·665 (0·015)	0·756 (0·021)

Sample:	FLZ13	DLZ7	DLZ14	DLZ10	DLZ8
P (GPa):	0·31	0·7	0·6	0·5	0·27
T (°C):	1100	1150	1000	1100	1100
No. An.:	9	11	5	16	9
SiO_2	50·40 (0·38)	53·10 (1·18)	51·20 (0·09)	48·80 (1·38)	47·90 (1·11)
TiO_2	0·06 (0·02)	0·10 (0·05)	0·04 (0·04)	0·03 (0·03)	0·05 (0·06)
Al_2O_3	31·90 (0·44)	29·10 (1·53)	30·10 (0·09)	32·70 (1·02)	30·90 (2·25)
Cr_2O_3	0·18 (0·03)	0·10 (0·07)	0·04 (0·07)	0·04 (0·04)	0·10 (0·09)
FeO	0·08 (0·04)	0·13 (0·12)	0·03 (0·06)	0·05 (0·17)	0·34 (0·48)
MgO	0·10 (0·12)	0·03 (0·04)	0·07 (0·09)	0·09 (0·25)	1·77 (2·27)
CaO	16·60 (0·23)	13·90 (0·76)	14·50 (0·10)	15·70 (0·56)	16·10 (1·82)
Na_2O	2·01 (0·12)	3·62 (0·46)	3·66 (0·07)	2·58 (0·40)	1·77 (0·35)
Total	101·33 (0·46)	100·00 (0·80)	99·64 (0·28)	99·98 (0·62)	98·93 (1·55)
Si	2·290 (0·023)	2·420 (0·055)	2·340 (0·005)	2·230 (0·062)	2·210 (0·040)
Ti	0·002 (0·001)	0·004 (0·002)	0·001 (0·001)	0·001 (0·001)	0·002 (0·002)
Al	1·710 (0·018)	1·560 (0·083)	1·620 (0·009)	1·760 (0·053)	1·680 (0·125)
Cr	0·007 (0·001)	0·004 (0·003)	0·001 (0·003)	0·001 (0·001)	0·004 (0·003)
Fe	0·003 (0·002)	0·005 (0·004)	0·001 (0·002)	0·000 (0·001)	0·012 (0·016)
Mg	0·007 (0·008)	0·002 (0·003)	0·005 (0·006)	0·006 (0·017)	0·121 (0·153)
Ca	0·806 (0·008)	0·681 (0·033)	0·711 (0·005)	0·770 (0·029)	0·799 (0·097)
Na	0·177 (0·011)	0·321 (0·041)	0·324 (0·006)	0·229 (0·035)	0·158 (0·030)
Cat·sum	5·001 (0·006)	4·996 (0·013)	5·004 (0·005)	4·998 (0·028)	4·985 (0·028)
(Na+Ca)	0·983 (0·004)	1·002 (0·044)	1·035 (0·002)	0·999 (0·025)	0·957 (0·069)
An	0·819 (0·011)	0·679 (0·032)	0·687 (0·006)	0·771 (0·033)	0·833 (0·043)

An = Ca/(Ca + Na). Numbers in parentheses correspond to 1σ standard deviations. Cations are calculated on the basis of 8 oxygens and all Fe = Fe^{2+}.

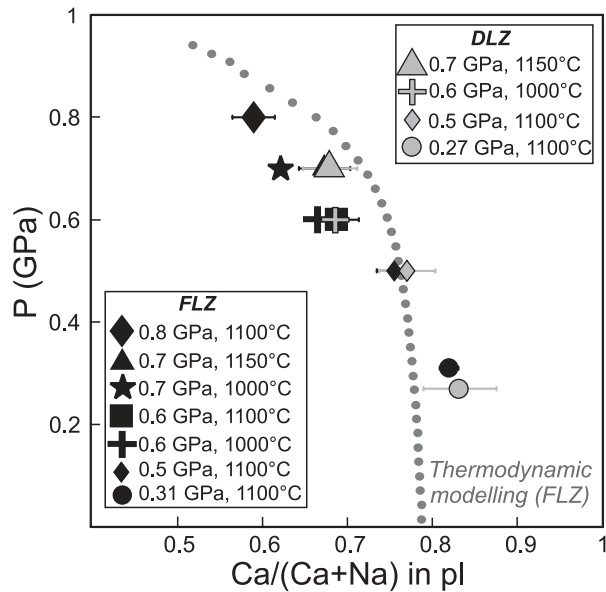**Fig. 5.** Variation of Ca/(Ca + Na) content in plagioclase vs pressure (GPa) in experiments on FLZ and DLZ compositions. Symbols as in Fig. 4. Experimental data are compared with Ca/(Ca + Na) variation in plagioclase (grey dotted curve), calculated at $T = 1100°C$ for the FLZ composition using Perple.X software (Connolly, 1990; Connolly & Petrini, 2002).

Cr–Al partitioning data resulting from this study are in excellent agreement with the available experimental data from similar peridotite compositions in complex chemical systems (Falloon *et al.*, 1997; Niida & Green, 1999; Wasylenki *et al.*, 2003; see Fig. 8).

X_{Cr} values of spinel and pyroxenes for FLZ at $P = 0.5–1.0$ GPa, $T = 1100°C$ were also calculated using the Perple.X package (Connolly, 1990; Connolly & Petrini, 2002), including the updated version of the Holland & Powell (1998) database and solid solution models for Cr-bearing pyroxenes, spinel and garnet (http://www.perplex.ethz.ch). When compared with the experimental data, thermodynamic modelling tends to severely underestimate the solubility of MgCrTs (Mg,Cr-Tschermak) and CaCrTs (Ca,Cr-Tschermak) in orthopyroxene and clinopyroxene, respectively, and consequently concentrates most Cr in spinel, as the Mg-chromite component. Consequently, calculated X_{Cr} values of pyroxenes are one order of magnitude lower than the X_{Cr} values of pyroxenes determined in the experiments, and the calculated X_{Cr} of spinel can be up to 0.3 higher than that derived experimentally (Fig. 8).

Phase abundances and quantification of the reaction

Phase abundances have been estimated by mass-balance calculations. As the ferric/ferrous ratio of each phase is unknown, all iron was treated as Fe^{2+}, although moderate amounts of Fe^{3+} are expected to be present in spinels.

Weighted least-squares minimization procedures were applied to balance the starting bulk composition with the average composition of each phase in the experiments. To take into account the fact that the system contains components with different variance, such as Na and Mg, different weights were assigned. The quality of the fit was evaluated on the basis of the sum of the squares of the residuals, where the residuals were calculated as the difference between the model starting composition and the bulk-composition calculated by considering the resulting phase proportions ($\sum R^2$; Table 8). In the fertile composition the sum of the squares of the residuals ranges between 0.10 and 0.21; in the depleted lherzolite higher values are found, especially for the spinel-facies assemblages. This is probably due to the uncertainty in the spinel compositions. Standard errors on the chemical analyses have been propagated to the phase abundances by the Monte Carlo method. Up to 10000 simulations normally distributed around the average value of each component of each phase have been evaluated and then statistically treated. Modal proportions (wt %) and propagated errors for FLZ–40% ol and DLZ–40% ol are reported in Table 8. In experiments conducted at 1000°C, where the fine-grained textures did not allow accurate analysis of spinel, mass-balance calculations were performed using the composition obtained in experiments at similar P–T conditions (e.g. for run FLZ14 at 0.6 GPa and 1000°C, the average spinel composition from run FLZ3 at 0.6 GPa and 1100°C was adopted).

Modal abundances, restored for the 40 wt % of olivine (Fo90) subtracted, are shown as a function of pressure at 1100°C in the FLZ experiments in Fig. 9a and at 1000–1100°C in the DLZ experiments in Fig. 9b. The depleted lherzolite has a higher olivine abundance (>63.6 ± 1.3 wt %) relative to the fertile lherzolite, as expected from the different Ca and Al contents in the two starting materials. In the fertile lherzolite, the higher Ca and Al contents maximize the clinopyroxene and plagioclase abundances with respect to orthopyroxene and olivine. Mass-balance calculations for both the FLZ and DLZ experiments indicate that the modal amount of plagioclase progressively decreases with increasing pressure up to the plagioclase-out boundary. This is coupled with a decrease in modal olivine and an increase in pyroxenes and spinel abundances, according to the continuous reaction

$$\text{plag} + \text{olivine} + \text{Al-poor px}_0 + \text{Cr-rich sp}_0$$
$$= \text{Al-rich sp}_1 + \text{Al-rich px}_1 \quad (8)$$
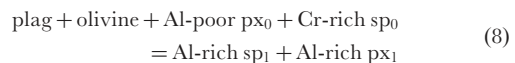
where sp_0 and px_0 refer to spinel and pyroxenes stable in the plagioclase stability field, characterized by Al-poor compositions, and sp_1 and px_1 are phases stable at spinel-facies conditions, which exhibit higher Al contents. Reaction (8) is mainly governed by the partitioning of Na–Ca and Cr–Al among the participating mineral phases.

Table 7: Representative compositions of spinels

Sample:	FLZ1	FLZ6	FLZ2	FLZ7	FLZ3
P (GPa):	1	0·9	0·8	0·7	0·6
T (°C):	1100	1100	1100	1150	1100
No. An.:	8	9	8	5	9
SiO$_2$	0·21 (0·34)	0·56 (0·39)	0·07 (0·09)	0·07 (0·06)	0·14 (0·11)
TiO$_2$	0·15 (0·04)	0·22 (0·03)	0·51 (0·11)	0·56 (0·03)	0·61 (0·02)
Al$_2$O$_3$	60·90 (0·90)	56·50 (1·72)	51·00 (1·57)	44·20 (0·59)	46·40 (2·37)
Cr$_2$O$_3$	7·65 (1·43)	10·80 (1·85)	18·00 (1·08)	23·60 (1·38)	20·80 (3·22)
FeO	9·68 (0·29)	8·05 (0·31)	10·60 (0·52)	11·40 (0·26)	11·40 (0·33)
MgO	20·80 (0·67)	21·30 (0·36)	19·40 (0·32)	19·50 (0·86)	20·30 (2·02)
Total	99·39 (0·55)	97·43 (0·61)	99·58 (0·60)	99·33 (0·31)	99·65 (0·39)
Si	0·005 (0·009)	0·015 (0·010)	0·002 (0·002)	0·002 (0·002)	0·004 (0·003)
Ti	0·003 (0·001)	0·004 (0·001)	0·010 (0·002)	0·012 (0·001)	0·012 (0·000)
Al	1·835 (0·024)	1·745 (0·037)	1·601 (0·039)	1·430 (0·016)	1·481 (0·055)
Cr	0·155 (0·029)	0·224 (0·040)	0·379 (0·025)	0·512 (0·031)	0·445 (0·075)
Fe	0·207 (0·007)	0·176 (0·006)	0·236 (0·012)	0·262 (0·007)	0·258 (0·013)
Mg	0·793 (0·024)	0·832 (0·010)	0·770 (0·015)	0·798 (0·029)	0·820 (0·064)
Cat·sum	2·997 (0·008)	2·996 (0·004)	2·998 (0·006)	3·015 (0·010)	3·020 (0·025)
X$_{Cr}$	0·078 (0·014)	0·114 (0·020)	0·191 (0·014)	0·264 (0·017)	0·231 (0·039)
X$_{Mg}$	0·793 (0·018)	0·825 (0·009)	0·765 (0·012)	0·753 (0·031)	0·760 (0·068)

Sample:	FLZ10	DLZ6	DLZ7	DLZ10	DLZ8
P (GPa):	0·5	0·9	0·7	0·5	0·27
T (°C):	1100	1100	1150	1100	1100
No. An.:	14	6	5	5	7
SiO$_2$	0·09 (0·12)	0·43 (0·21)	0·00 (0·00)	0·14 (0·11)	0·00 (0·00)
TiO$_2$	0·76 (0·05)	0·20 (0·05)	0·30 (0·02)	0·39 (0·02)	0·40 (0·05)
Al$_2$O$_3$	43·00 (1·59)	51·20 (0·42)	35·60 (0·41)	46·90 (1·67)	32·50 (0·61)
Cr$_2$O$_3$	26·50 (1·45)	16·50 (0·70)	34·50 (0·96)	20·90 (1·68)	39·40 (1·24)
FeO	12·30 (0·35)	8·61 (0·39)	9·92 (0·41)	11·80 (0·28)	9·15 (0·77)
MgO	17·40 (0·55)	21·90 (0·28)	20·89 (0·58)	20·70 (0·09)	18·50 (0·63)
Total	100·05 (1·02)	98·84 (0·40)	101·21 (0·57)	100·82 (0·19)	99·95 (0·54)
Si	0·003 (0·003)	0·011 (0·005)	0·000 (0·000)	0·004 (0·003)	0·000 (0·000)
Ti	0·016 (0·001)	0·004 (0·001)	0·006 (0·000)	0·008 (0·000)	0·009 (0·001)
Al	1·398 (0·041)	1·598 (0·009)	1·196 (0·012)	1·481 (0·046)	1·094 (0·018)
Cr	0·578 (0·033)	0·345 (0·016)	0·777 (0·024)	0·443 (0·038)	0·890 (0·032)
Fe	0·284 (0·011)	0·191 (0·006)	0·272 (0·013)	0·264 (0·007)	0·219 (0·016)
Mg	0·715 (0·016)	0·864 (0·008)	0·756 (0·023)	0·827 (0·008)	0·788 (0·023)
Cat·sum	2·994 (0·006)	3·013 (0·004)	3·007 (0·007)	3·027 (0·001)	2·999 (0·013)
X$_{Cr}$	0·292 (0·018)	0·178 (0·009)	0·394 (0·012)	0·230 (0·019)	0·449 (0·014)
X$_{Mg}$	0·716 (0·012)	0·819 (0·012)	0·790 (0·022)	0·758 (0·011)	0·783 (0·017)

$X_{Cr} = Cr/(Cr + Al)$; $X_{Mg} = Mg/(Mg + Fe^{tot})$. Numbers in parentheses correspond to 1σ standard deviations. Cations are calculated on the basis of 4 oxygens and all $Fe = Fe^{2+}$.
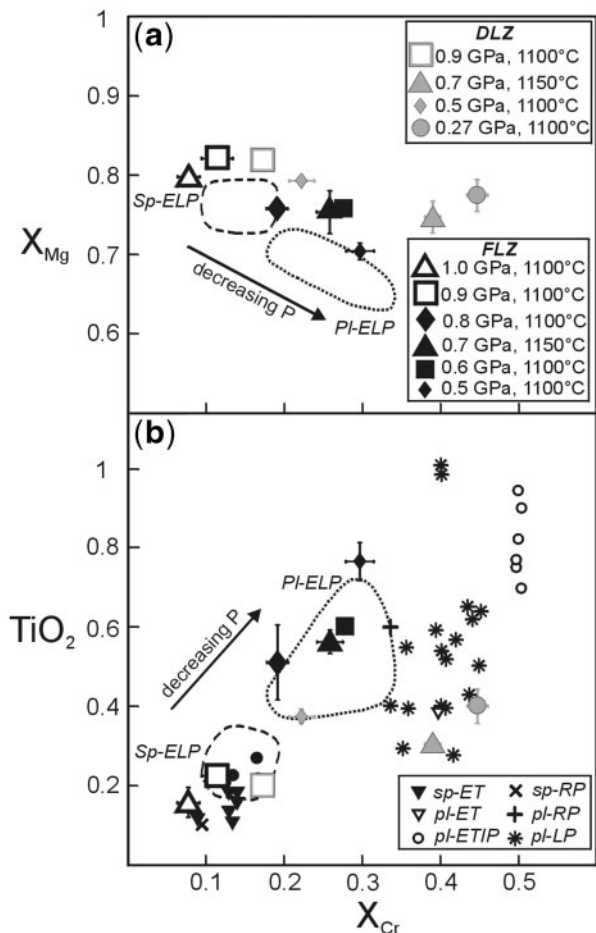
Fig. 6. (a) X_{Cr} value [$X_{Cr} = Cr/(Cr + Al)$] vs X_{Mg} value [$X_{Mg} = Mg/(Mg + Fe^{tot})$] of spinels from the experiments on FLZ and DLZ. Run symbols are as in Fig. 4: open and filled symbols refer to plagioclase-free and plagioclase-bearing experiments, respectively. Also reported are the compositional fields of spinels from spinel-facies (dashed field) and plagioclase-facies (dotted field) assemblages in the External Liguride peridotites (ELP; Northern Apennines, Italy; Borghini, 2008). (b) X_{Cr} value vs TiO_2 (wt %) content of spinels in the FLZ and DLZ experiments. Compositional fields as in (a). Also reported are the compositions of spinels in spinel peridotites and equilibrated plagioclase peridotites from the Ronda (Betic Cordillera, southern Spain, *sp-RP* and *pl-RP*; Obata, 1980) and Erro–Tobbio massifs (Ligurian Alps, Italy, *sp-ET* and *pl-ET*; Rampone *et al.*, 2005; Piccardo & Vissers, 2007), together with spinels in impregnated plagioclase peridotites from Lanzo Nord (Western Alps, *pl-LP*; Kaczmarek & Müntener, 2008) and Erro–Tobbio (*pl-ETIP*, Piccardo & Vissers, 2007; Borghini *et al.*, 2007). (See text for further details.)

In the simple system NCMAS the upper pressure stability of plagioclase is constrained by reactions (1) and (3), delimiting the five-phase mineral assemblage. This implies that the persistence of plagioclase is not only a function of its composition (i.e. that albite-rich plagioclase will be favoured at higher pressure) but also that its upper pressure stability is moderated by the presence and modal abundance of clinopyroxene, as a relevant host for the jadeite molecule (Green & Hibberson, 1970). A powerful
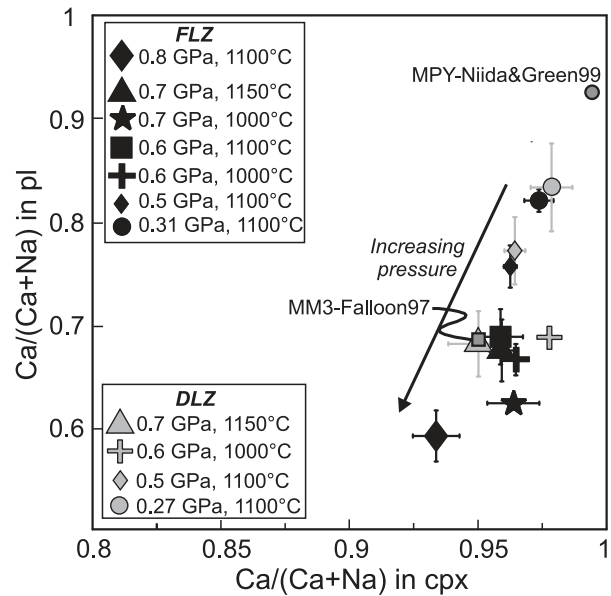
Fig. 7. Ca/(Ca + Na) partitioning between clinopyroxene (cpx) and plagioclase (pl) Symbols as in Fig. 5. For comparison, we have reported experimental data from (1) Niida & Green (1999) on MORB pyrolite in a hydrous complex system (at 0·5 GPa and 925°C), and (2) Falloon *et al.* (1997) on MM3 lherzolite in a complex system (at 1·0 GPa and 1250°C).

way to explore this effect is through the bulk-rock Ab/Di normative ratio, expecting that the higher the ratio, the higher the upper pressure stability of plagioclase.

Reaction (8) is also controlled by Cr–Al partitioning between spinel and pyroxenes, according to the following reactions, modelled in the simple CrCMAS system:

$$MgCr_2O_4 + 2CaAl_2Si_2O_8 + 2Mg_2SiO_4$$
Mg-chromite   anorthite   forsterite
$$= MgAl_2O_4 + 2MgCrAlSiO_6 + 2CaMgSi_2O_6 \quad (9)$$
spinel   MgCrTs   diopside

$$MgCr_2O_4 + 2CaAl_2Si_2O_8 + 2Mg_2SiO_4$$
Mg-chromite   anorthite   forsterite
$$= MgAl_2O_4 + 2CaCrAlSiO_6 + 2Mg_2Si_2O_6 \quad (10)$$
spinel   CaCrTs   enstatite
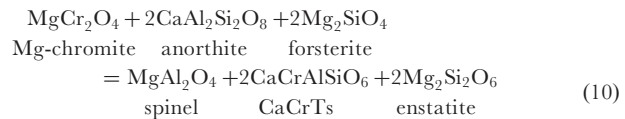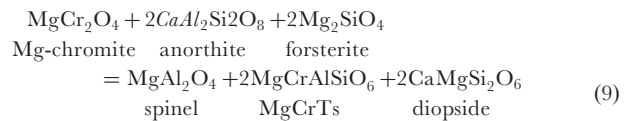
This implies that the Cr–Al partitioning between spinel and pyroxenes is complicated by the contribution of plagioclase as follows:

$$MgCr_2O_4 + CaAl_2Si_2O_8$$
Mg-chromite   anorthite
$$= MgCrAlSiO_6 + CaCrAlSiO_6 \quad (11)$$
MgCrTs   CaCr-Ts
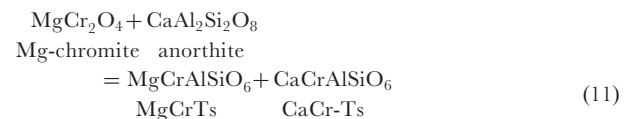
As a result, at fixed *P–T* conditions, the X_{Cr} of spinel is not only dependent on the X_{Cr} of the bulk composition but is also correlated with the presence and abundance of plagioclase. The normative Cm/An ratio of the bulk composition therefore represents a valid parameter to predict the effect
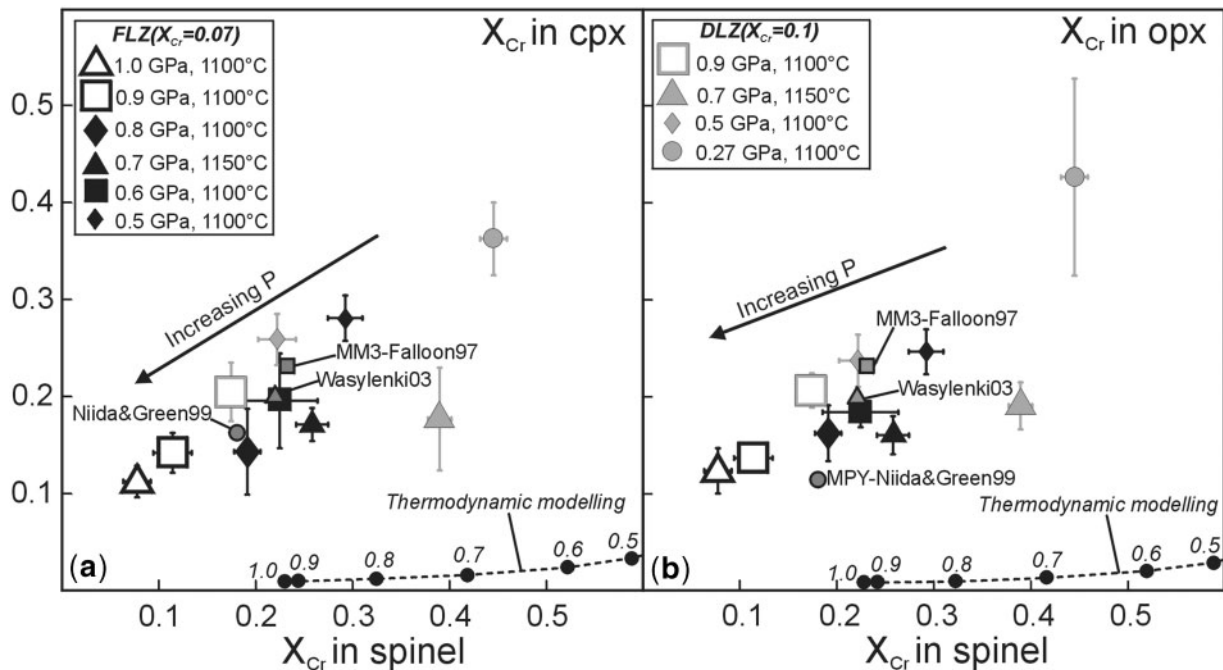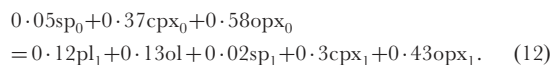
Fig. 8. Cr–Al partitioning between spinel $[X_{Cr} = Cr/(Cr + Al)]$ and clinopyroxene (a) and orthopyroxene (b) $[X_{Cr} = Cr/(Cr + Al^{VI})]$ from experiments on FLZ and DLZ (the bulk X_{Cr} value is reported in parentheses) and previous experimental studies performed in complex chemical systems on MORB pyrolite (at 1·0 GPa and 925°C; Niida & Green, 1999), MM3 lherzolite (at 1·0 GPa and 1250°C; Falloon *et al*. 1997), and DMM1 depleted lherzolite (at 1·0 GPa and 1250°C; Wasylenki *et al*., 2003). Filled black circles connected by dashed lines represent the spinel–pyroxene X_{Cr} variation trends calculated at P from 0·5 to 1·0 GPa and $T = 1100$°C for the FLZ composition, using PerpleX software (Connolly, 1990; Connolly & Petrini, 2002) in the Cr-NCFMAS system (see text for further details).

of Cr–Al partitioning on the upper pressure stability of plagioclase (see the discussion below).

Mass-balance calculations using the average mineral compositions in experiments at P–T conditions across the transition between plagioclase and spinel lherzolite (runs FLZ6 and FLZ2 respectively; see Tables 3–7) allowed us to quantify the stoichiometric coefficients of the reaction for the FLZ bulk. The results yielded the following balanced reaction:

$$0 \cdot 05 sp_0 + 0 \cdot 37 cpx_0 + 0 \cdot 58 opx_0$$
$$= 0 \cdot 12 pl_1 + 0 \cdot 13 ol + 0 \cdot 02 sp_1 + 0 \cdot 3 cpx_1 + 0 \cdot 43 opx_1. \quad (12)$$

Rampone *et al*. (1993) quantified the plagioclase–spinel lherzolite reaction by mass balance using the mineral chemistry variations observed in the External Liguride peridotites. Although they did not consider Cr-spinel as a product phase, their results are in agreement with the experimentally based results represented by reaction (12).

In summary, the results of experiments within the plagioclase stability field indicate that the plagioclase–spinel lherzolite transition is a continuous reaction marked by systematic modal and chemical changes in the constituent minerals. At increasing P, modal plagioclase decrease is coupled with an increase in modal pyroxenes and spinel; these variations are correlated with a progressive decrease

of the anorthite content in plagioclase and Cr, Ti in spinel, in turn coupled with an Al content increase in both spinel and pyroxenes (Figs 4, 5 and 6a,b).

The plagioclase-out boundary in lherzolite compositions

The experimental results of this study indicate that the plagioclase-out boundary in the fertile lherzolite FLZ occurs between 0·8 and 0·9 GPa at 1100°C, and between 0·7 and 0·8 GPa at 1000°C. The complexity of the chemical system and the bulk composition adopted in the experiments strongly affect the position of the plagioclase-out reaction, as suggested by the Na–Ca and Cr–Al partitioning among phases. When compared with available experimental results for fertile lherzolites, modelled in different complex chemical systems (Fig. 10a), the bulk composition dependence finds further confirmation. Despite good agreement regarding the positive dP/dT slope of the transition, the pressure at which plagioclase disappears varies from 0·8 to 1·5 GPa (Kushiro & Yoder, 1966; Green & Hibberson, 1970; Green & Ringwood, 1970; Green & Falloon, 1998; Niida & Green, 1999; Presnall *et al*., 2002).

In CMAS, the univariant plagioclase–spinel transition occurs at $T = 1100$°C and a pressure of about 0·7 GPa for the 2Fo + 1An composition (Fig. 10a, curve 3; Kushiro &

Table 8: Phase proportions (in wt %) in experiments calculated by weighted mass balance

Run	P	T	Data relative to FLZ and DLZ −40% olivine					$\sum R^{2*}$	Data with 40% olivine restored				
	(GPa)	(°C)	ol	opx	cpx	plag	sp		ol	opx	cpx	plag	sp
FLZ1	1·0	1100	30·8 (2·0)	38·5 (2·7)	27·1 (0·9)	—	3·6 (0·4)	0·02	58·5 (1·2)	23·1 (1·6)	16·3 (0·5)	—	2·2 (0·2)
FLZ6	0·9	1100	29·5 (2·3)	40·7 (2·8)	26·1 (0·8)	—	3·6 (0·5)	0·21	57·7 (1·4)	24·4 (1·7)	16·0 (0·5)	—	2·2 (0·3)
FLZ2	0·8	1100	36·7 (2·6)	32·1 (3·3)	21·2 (1·3)	8·0 (0·9)	2·0 (0·4)	0·03	62·0 (1·6)	19·3 (2·0)	12·7 (0·8)	4·8 (0·6)	1·2 (0·2)
FLZ12	0·8	1000	28·9 (2·0)	40·7 (3·0)	26·2 (1·2)	—	4·1 (0·4)	0·07	57·4 (1·2)	24·4 (1·8)	15·7 (0·8)	—	2·5 (0·2)
FLZ7	0·7	1150	41·9 (2·9)	27·8 (3·7)	18·3 (1·3)	10·0 (1·1)	2·0 (0·2)	0·02	65·2 (1·8)	16·7 (2·2)	11·0 (0·8)	6·0 (0·6)	1·2 (0·1)
FLZ5	0·7	1000	40·3 (2·4)	29·3 (2·9)	19·1 (0·7)	9·7 (0·6)	1·6 (0·2)	0·04	64·2 (1·5)	17·6 (1·8)	11·4 (0·4)	5·8 (0·4)	1·0 (0·1)
FLZ3	0·6	1100	42·1 (3·2)	27·6 (3·5)	16·9 (1·1)	12·1 (1·3)	1·2 (0·4)	0·03	65·2 (1·9)	16·6 (2·1)	10·2 (0·7)	7·3 (0·8)	0·7 (0·3)
FLZ14	0·6	1000	39·7 (2·6)	29·3 (3·4)	17·8 (1·4)	11·7 (0·9)	1·5 (0·3)	0·04	63·8 (1·6)	17·6 (2·1)	10·7 (0·9)	7·0 (0·6)	0·9 (0·2)
FLZ10	0·5	1100	42·9 (2·6)	26·3 (3·1)	16·3 (1·1)	13·5 (0·9)	1·0 (0·3)	0·01	65·8 (1·6)	15·8 (1·9)	9·8 (0·6)	8·1 (0·5)	0·6 (0·2)
FLZ13	0·31	1100	43·4 (2·3)	25·8 (2·7)	14·9 (1·1)	14·7 (0·6)	1·1 (0·4)	0·03	66·1 (1·4)	15·5 (1·6)	9·0 (0·7)	8·8 (0·3)	0·7 (0·2)
DLZ6	0·9	1100	39·3 (2·1)	45·0 (2·5)	13·8 (0·4)	—	1·9 (0·3)	0·83	63·6 (1·3)	27·0 (1·5)	8·3 (0·3)	—	1·2 (0·2)
DLZ12	0·8	1000	41·1 (1·8)	43·8 (2·2)	13·0 (0·3)	—	2·1 (0·2)	0·59	64·7 (1·1)	26·3 (1·3)	7·8 (0·2)	—	1·2 (0·1)
DLZ7	0·7	1150	46·4 (2·6)	37·3 (3·1)	10·2 (1·0)	5·4 (0·8)	0·7 (0·1)	0·15	67·8 (1·6)	22·4 (1·9)	6·1 (0·6)	3·2 (0·5)	0·4 (0·1)
DLZ5	0·7	1000	43·3 (1·9)	41·1 (2·3)	13·5 (0·5)	—	2·1 (0·2)	0·17	66·0 (1·2)	24·6 (1·4)	8·1 (0·3)	—	1·3 (0·1)
DLZ14	0·6	1000	44·3 (1·9)	39·1 (2·2)	9·9 (0·5)	5·9 (0·4)	0·8 (0·3)	0·19	66·6 (1·1)	23·5 (1·3)	5·9 (0·3)	3·6 (0·3)	0·5 (0·2)
DLZ10	0·5	1100	46·3 (2·4)	36·7 (2·6)	9·8 (0·7)	6·7 (0·4)	0·5 (0·2)	0·22	67·8 (1·4)	22·0 (1·6)	5·9 (0·4)	4·0 (0·3)	0·3 (0·1)
DLZ8	0·27	1100	47·1 (2·8)	35·1 (3·5)	9·0 (1·3)	8·3 (0·9)	0·5 (0·2)	0·49	68·3 (1·7)	21·1 (2·1)	5·4 (0·8)	5·0 (0·6)	0·3 (0·1)

*Sum of the squares of the residuals for all elements calculated as the sum of the squares of the difference between model and calculated composition.
ol, olivine; opx, orthopyroxene; cpx, clinopyroxene; pl, plagioclase; sp, spinel. Numbers in parentheses are propagated errors from Monte Carlo simulations. Phase proportions for fertile and depleted lherzolites have been recalculated by restoring the 40% of olivine, to refer to the original composition of FLZ and DLZ. Modal amounts resulting from mass balance have been normalized to 60%, and then 40% of olivine has been added. This introduces a negligible error, as olivine does not show large compositional variations in experiments with respect to the model olivine subtracted *a priori* (see Table 1).

Yoder, 1966), and is extrapolated from near-solidus experiments at about 0·9 GPa for LherzA bulk (curve 4; Presnall *et al.*, 1979). Presnall and co-workers documented that the addition of Na and Fe has the same effect, moving the plagioclase-out reaction toward higher pressure (e.g. curve 5; NCMAS, Walter & Presnall, 1994; FCMAS, Gudfinnsson & Presnall, 2000; Fig. 10a). Our experiments on FLZ and DLZ in Ti,Cr-NCFMAS locate the plagioclase breakdown boundary at lower pressure than in NCMAS and FCMAS (respectively curves 1 and 2 in Fig. 10a). This discrepancy is presumably due to the presence of Cr in our bulk system, as Cr is expected to control plagioclase + forsterite reactions by lowering the pressure of plagioclase stability [reactions (8) and (9)]. A similar result has been recently documented by Keshav *et al.* (2008) based on near-solidus or solidus experiments in the CrCMAS system.

Interesting indications of the effect of bulk composition on subsolidus plagioclase lherzolite stability can be deduced from comparison of our results with experimental results on pyrolite-type compositions (see Table 1).

Green & Ringwood (1970) located the plagioclase-out boundary in Hawaiian pyrolite (HPY) at 0·9–1·0 GPa and 1000–1100°C (curve 6, Fig. 10a); that is, at a pressure 0·2 GPa higher than in FLZ. Similar results were obtained by Niida & Green (1999) for MORB pyrolite (MPY) in a hydrous complex system (curve 7, Fig. 10a). This pressure discrepancy is probably due to the higher Na content in 'Hawaiian' and 'MORB' pyrolites relative to FLZ, reflecting significantly higher Ab/Di normative ratios (see Table 1). This supports the already known striking dependence of the plagioclase upper pressure stability on bulk composition, specifically the Na_2O/CaO ratio and normative plagioclase content (Gasparik, 1987; Walter & Presnall, 1994; Falloon *et al.*, 2008). Moreover, experiments on pyrolite compositions (Green & Falloon, 1998, and references therein) indicate that more depleted compositions (i.e. with lower bulk Na_2O/CaO and Ab/Di normative ratios) are expected to encounter the appearance of plagioclase at lower pressure.

Our experiments indicate that in the depleted lherzolite DLZ the plagioclase-out boundary occurs between 0·7
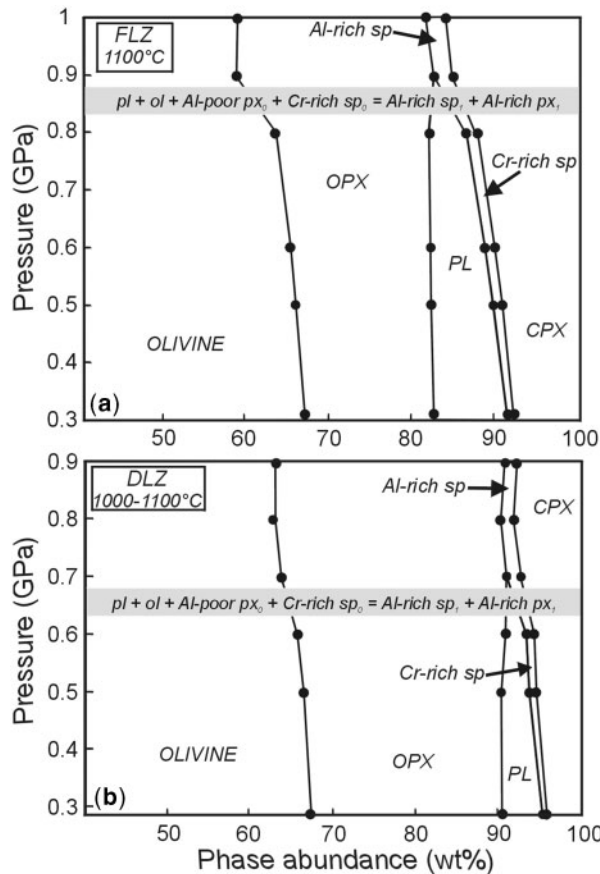
Fig. 9. Modal abundances restored with addition of 40% olivine in FLZ at 1100°C (a), and in DLZ at 1000–1100°C (b), calculated by mass balance as a function of pressure. The grey bands represent the pressure range in which the plagioclase-bearing assemblage disappears.
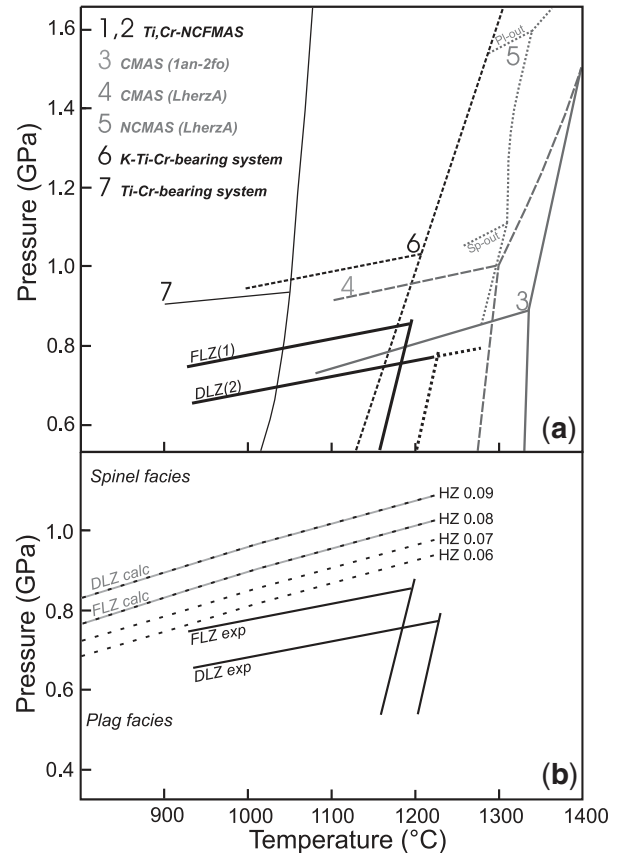

Fig. 10. (a) The plagioclase-out boundary and solidus curves resulting from this experimental study (FLZ: reaction curve 1; DLZ: reaction curve 2) compared with existing experimental data on: (curve 3) 2:1 fosterite–anorthite assemblage from Kushiro & Yoder (1966), (curve 4) model lherzolite in the CMAS system from Presnall *et al.* (1979); (curve 5) model lherzolite in the NCMAS system from Walter & Presnall (1994); (curve 6) 'Hawaiian' pyrolite modelled in the complex K,Cr,Ti-bearing system from Green & Ringwood (1970); (curve 7) 'MORB' pyrolite modelled in a hydrous Cr,Ti-bearing system from Niida & Green (1999). (b) The experimentally derived plagioclase-out boundaries (FLZ exp and DLZ exp) are compared with those derived by thermodynamic calculation using the Perple_X package (Connolly, 1990; Connolly & Petrini, 2002) in the model system Cr-NCFMAS (FLZ calc and DLZ calc, grey curves). The black dashed curves refer to plagioclase-out boundaries calculated for a harzburgite composition (HZ; see text for further details) assuming different Na_2O/CaO ratios varying from 0·06 to 0·09.

and 0·8 GPa at 1100°C, and it is shifted towards lower P (by about 0·1 GPa) relative to FLZ (Fig. 10a). Despite different absolute bulk Na_2O, CaO and Al_2O_3 contents, FLZ and DLZ have similar Na_2O/CaO ratios and similar Ab/Di normative ratios. On the other hand, DLZ has a higher X_{Cr} value and Cm/An ratio relative to FLZ (Table 1). As discussed above, plagioclase disappearance is strongly driven by Cr–Al partitioning between spinel and pyroxenes. Although plagioclase does not host Cr, it participates in the reactions producing Mg,Cr-Tschermak and Ca,Cr-Tschermak in pyroxenes and in consuming Mg-chromite in spinel [reactions (9)–(11)]. As a result, bulk compositions with higher Cm/An normative ratios would account for spinel with a higher X_{Cr} value and, therefore, would encounter the plagioclase-out boundary at progressively lower pressures. Our experimental results thus confirm this bulk X_{Cr} value effect, indicating that at similar Na_2O/CaO ratios (and similar bulk Ab/Di), an increase of 0·03 in the bulk X_{Cr}, corresponding to an increase of 0·05 in the Cm/An ratio (see Table 1), accounts

for about a 0·1 GPa lowering in the pressure of plagioclase disappearance (Fig. 10a).

To evaluate the dependence of the bulk-rock chemistry on the location of the boundary between plagioclase lherzolite and spinel lherzolite, we computed pseudosections using the Perple_X package (Connolly, 1990; Connolly & Petrini, 2002). The results suggest that the P–T location of this boundary obtained by thermodynamic modelling is solely sensitive to the bulk-rock Na_2O/CaO ratio, despite different bulk-rock X_{Cr} values. As illustrated in Fig. 10b,
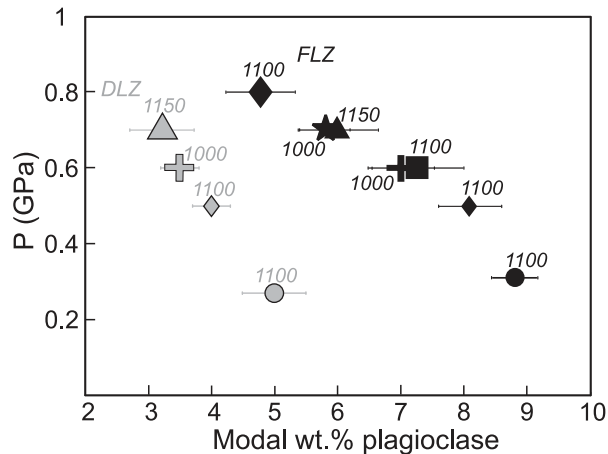
Fig. 11. Variation of the plagioclase modal abundance as a function of pressure derived from experiments on FLZ and DLZ. Symbols as in Fig. 5. Plagioclase amounts were restored with addition of 40% olivine (see Table 8). Labels close to symbols indicate the temperature of each experimental run.

the modelled plagioclase-out reaction for the depleted composition DLZ is placed at higher P than the computed reaction curve for FLZ; this is due to the slightly higher Na_2O/CaO ratio (and slightly higher Ab/Di ratio) in DLZ (Table 1) and is inconsistent with the experimental results. To further check the strict dependence of computed transitions on the Na_2O/CaO value, calculations were also performed on a depleted harzburgite composition ($X_{Mg} = 0.91$; $X_{Cr} = 0.12$; $Al_2O_3 = 1.53$ wt %; $CaO = 1.61$ wt %) using different Na_2O contents to model different Na_2O/CaO ratios. We found that, for harzburgite with an Na_2O/CaO ratio equal to those of FLZ and DLZ, the resulting reaction curves exactly overlap the reactions calculated assuming the original FLZ and DLZ compositions (Fig. 10b). This confirms that thermodynamic modelling of the plagioclase-out boundary in $P–T$ space accounts for only the Na_2O/CaO ratio, but fails to predict the effect of bulk depletion in terms of X_{Cr}.

Figure 10b additionally reveals that the modelled breakdown of plagioclase for FLZ is located at pressure about 0.2 GPa higher than the experimentally derived curve (Fig. 10b). Thermodynamic calculations on the FLZ composition have provided information about the Ca–Na partitioning in plagioclase and Al solubility in pyroxenes, consistent with the experimental results (see Figs 4 and 5), whereas the Cr partitioning between spinel and pyroxenes is not correctly reproduced (see Fig. 8 and discussion above). Therefore, the observed unrealistic shift towards higher pressure of the modelled plagioclase-out boundary in FLZ is presumably due to the overestimation of the Cr content in spinel, confirming that Cr partitioning has an important role in plagioclase stability in mantle peridotites.

Chemistry and modal abundance of plagioclase in lherzolite compositions

The results of this study indicate that plagioclase chemistry, in a given bulk composition, is strongly sensitive to pressure and varies significantly in a rather narrow pressure range (in FLZ: $An = 0.83–0.59$ at P ranging from 0.31 to 0.8 GPa). On the other hand, experiments at similar $P–T$ conditions on different bulk compositions provide evidence that, despite its strong P dependence, Ca–Na partitioning between plagioclase and clinopyroxene is not significantly affected by the bulk composition (Fig. 7). As a consequence, at the same $P–T$ conditions, plagioclase chemistry is similar in both FLZ and DLZ (Fig. 5).

The two lherzolite compositions investigated in this study, although having different X_{Cr} values, have similar Na_2O/CaO ratio (or Ab/An normative ratios); therefore, our experimental results cannot rule out a possible effect of the bulk Na_2O/CaO on the plagioclase chemistry. Green & Falloon (1998) documented that different plagioclase compositions in HPY, MPY and Tinaquillo (TQ) depleted lherzolites (with progressively lower Na_2O/CaO ratios) reflect differences in the location of the subsolidus plagioclase-out boundary, so that the An content in plagioclase near the plagioclase-out reaction is progressively higher from more fertile HPY to depleted TQ. However, Green & Falloon (1998) did not report experimental data on plagioclase composition in the different bulk compositions at the same $P–T$ conditions. In the light of available experimental results (Green & Falloon, 1998; this study), we could speculate that the bulk composition exerts a strong influence on the high-pressure stability of the plagioclase lherzolite mineral assemblage (see discussion above), but that it has a minor effect on the chemistry of the plagioclase at fixed $P–T$ conditions. This would make the plagioclase composition a powerful geobarometric marker of low-P re-equilibration in mantle peridotites. Parallel detailed chemical investigations of plagioclase peridotites from various natural occurrences, combined with the experimental results from this study, have confirmed this prediction (Borghini *et al.*, in preparation). However, further experimental studies on lherzolites with variable alkali contents are needed, to test the existence of a correlation between plagioclase chemistry and bulk-rock Na_2O/CaO ratio, thus enlarging the potential for developing a plagioclase geobarometer applicable to mantle peridotites (work in progress).

In the investigated FLZ and DLZ compositions, similar plagioclase compositions at fixed $P–T$ conditions are balanced by different plagioclase and clinopyroxene modal proportions (Table 8). The modal amount of plagioclase progressively decreases with increasing pressure up to the plagioclase-out boundary; in FLZ, plagioclase abundance at 1100°C varies from 8.8 wt % at 0.31 GPa to

4·8 wt % at 0·8 GPa, whereas in DLZ plagioclase is less abundant, ranging from 5·0 wt % at 0·27 GPa and 1100°C to 3·2 wt % at 0·7 GPa and 1150°C (Fig. 11). These modal estimates, resulting from the continuous reaction in the complex system Ti,Cr-NCFMAS, are significantly lower than the amounts of plagioclase predicted by the simplified reactions that are commonly adopted in modelling the phase equilibria that control the mineralogy of the uppermost lithospheric mantle (e.g. Wood & Yuen, 1984; Simon & Podladchikov, 2008). Simple parameterization is based on mineral end-member reactions, which ignore the solubility of Al in pyroxenes and Cr-bearing spinel and concentrate all the Al_2O_3 in plagioclase, thus leading to an overestimation of the plagioclase abundance. As an example, adopting the model reaction proposed by Simon & Podladchikov (2008) and assuming, as suggested by the experimental results, that plagioclase of An_{59} and An_{68} composition forms respectively in FLZ and DLZ at near-transition conditions (0·8 GPa, 1100°C in FLZ and 0·7 GPa, 1150°C in DLZ), the resulting plagioclase abundance is 13 and 10 wt % respectively; such values are much higher than the modal plagioclase estimates for the FLZ and DLZ experiments (about 5 and 3 wt % respectively; see Fig. 11). It should also take into account that the plagioclase modal amounts resulting from the experiments probably constitute an overestimate with respect to natural occurrences, where low-P recrystallization is generally confined to discrete microstructural domains between spinel-facies porphyroclastic minerals (Obata, 1980; Hoogerduijn Strating et al., 1993; Rampone et al., 1993, 1995, 2005; Cannat et al., 1995; Ozawa & Takahashi, 1995; Takazawa et al., 1996; Fabries et al., 1998; Newman et al., 1999; Montanini et al., 2006).

Our experimental study thus provides a reliable quantification of the maximum plagioclase budget produced by subsolidus low-P recrystallization in peridotites with lherzolitic compositions over a wide range defined by natural mantle rocks. These are about 9 wt % (at 0·31 GPa) in a fertile lherzolite (FLZ), and 5 wt % (at 0·27 GPa) in a depleted lherzolite (DLZ) (see Fig. 11), slightly lower than the ideal maximum amount of plagioclase indicated by CIPW norms (11·4 and 7·3 wt % respectively in FLZ and DLZ). Higher plagioclase abundances are expected only in very fertile lherzolites, probably refertilized by percolating melts.

The composition of spinel in plagioclase-bearing mantle assemblages

Compositional variations in spinel from our experiments are strongly correlated with pressure; that is, X_{Mg} decreases and X_{Cr} and TiO_2 increase with decreasing P. Such chemical changes are overall consistent with those documented in many spinel and plagioclase peridotites from natural occurrences (see Fig. 6a and b).

Chromium enrichment (X_{Cr} increase) coupled with X_{Mg} decrease has been largely documented in spinels from both metamorphic (Obata, 1980; Woodland et al., 1992; Rampone et al., 1993, 2005; Cannat & Seyler, 1995; Newman et al., 1999) and impregnated plagioclase peridotites (Dick & Bullen, 1984; Seyler & Bonatti, 1997; Müntener et al., 2005; Müntener & Manatschal, 2006; Borghini et al., 2007; Piccardo & Vissers, 2007; Rampone et al., 2008). On the other hand, Ti enrichment in spinels from plagioclase peridotites is largely considered as an indicator of melt–rock interaction, because high Ti contents are believed to derive from equilibration with melts. This has been inferred for abyssal peridotites (Dick & Bullen, 1984; Dick, 1989; Seyler & Bonatti, 1997; Hellebrand et al., 2002; Tartarotti et al., 2002), as well as impregnated plagioclase peridotites from ophiolitic massifs (Rampone et al., 1997; Piccardo & Vissers, 2007; Piccardo et al., 2007; Kaczmarek & Müntener, 2008; Rampone et al., 2008) (see Fig. 6b). Ti enrichment in spinel has also been documented in equilibrated plagioclase peridotites inferred to be of metamorphic origin (Obata, 1980; Kornprobst & Tabit, 1988; Rampone et al., 1993, 2005, 2008; Cannat & Seyler, 1995; Borghini, 2008) (see Fig. 6b), and has been considered to be a result of the fact that titanium does not enter plagioclase and olivine, but rather is partitioned into newly formed spinel and pyroxene (Kornprobst & Tabit, 1988; Rampone et al., 1993).

Our experimental study indicates that, in the plagioclase stability field, Ti is partitioned exclusively between spinel and pyroxenes. With decreasing pressure, a Ti increase in spinel is coupled with a decrease in its modal amount; at fixed P–T conditions, the Ti abundance in spinel is controlled by the ilmenite (Il) normative content of the bulk composition (see Table 1). Constant low Ti contents in both pyroxenes with P–T variation (Tables 4 and 5) suggest that Ti is preferentially concentrated in spinel. Moreover, very low TiO_2 contents in pyroxenes at 1000°C could indicate a temperature dependence of Ti partitioning between spinel and pyroxenes, although the lack of reliable spinel analyses in experiments at $T < 1100$°C cannot unequivocally confirm this hypothesis.

The low-P recrystallization at plagioclase-facies conditions leads to rather high TiO_2 abundances in spinel, even in a depleted lherzolite (TiO_2 content in spinel up to 0·4 wt % in DLZ at 0·27 GPa; see Fig. 6b) with a low bulk TiO_2 content of 0·07 wt % (see DLZ in Table 1). This suggests careful evaluation of the Ti content of spinel as an indicator of melt entrapment. It must be emphasized, however, that in our experiments we did not observe the very high TiO_2 abundances (>1 wt %) that have occasionally been found in spinels from some impregnated plagioclase peridotites (Borghini et al., 2007; Piccardo & Vissers, 2007; Kaczmarek & Müntener, 2008; see Fig. 6b).

CONCLUDING REMARKS

(1) Subsolidus experiments on lherzolitic mantle compositions in the Ti,Cr-NCFMAS system indicate that the maximum pressure at which plagioclase is stable in a fertile lherzolite (FLZ, $Na_2O/CaO = 0.08$; $X_{Cr} = 0.07$) is 0.8–0.7 GPa, at 1100–$1000°C$, with the plagioclase- to spinel-facies transition having a positive slope in P–T space. The stability of the plagioclase lherzolite assemblage is shifted toward lower pressure (0.6 GPa) in a depleted lherzolite (DLZ, $Na_2O/CaO = 0.09$; $X_{Cr} = 0.10$).

(2) In lherzolites with similar Ab/Di normative ratio (or similar bulk Na_2O/CaO ratios), the pressure of plagioclase disappearance is affected by the X_{Cr} of spinel, which is in turn controlled by the solubility of the Mg,Cr-Tschermak and Ca,Cr-Tschermak components in pyroxenes, according to the reaction Mg-chromite + anorthite = Mg,Cr-Tschermak + Ca,Cr-Tschermak. Consequently, the high-pressure stability of the plagioclase lherzolite mineral assemblage depends on the X_{Cr} and chromite/anorthite normative ratio of the bulk composition. When compared with experimental data, thermodynamic modelling yields incorrect spinel–pyroxene Cr–Al partitioning, thus resulting in unreliable estimates of the P–T location of the plagioclase-out boundary. Thus, our work provides new constraints for the stability of plagioclase in mantle peridotites as a function of the bulk composition.

(3) Within the plagioclase stability field, systematic compositional variations in minerals occur with decreasing pressure; for example, an Al decrease in pyroxenes coupled with an anorthite increase in plagioclase and a Ti and X_{Cr} increase in spinel. Chemical variations in minerals are accompanied by modal changes. The plagioclase modal amount increases progressively with decreasing pressure, and is coupled with a modal olivine increase and a pyroxene and spinel decrease, in response to a continuous reaction. The highest plagioclase modal abundances have been found in experiments at the lowest pressures, about 9 wt % in FLZ (at 0.31 GPa) and 5 wt % in DLZ (at 0.27 GPa).

(4) Experimental results on FLZ and DLZ indicate that the bulk composition exerts a strong influence on the high-pressure stability of the plagioclase lherzolite assemblage, but that it has a minor effect on Na–Ca partitioning between plagioclase and clinopyroxene, and the chemistry of plagioclase, at fixed P–T conditions. On the other hand, plagioclase chemistry is very sensitive to pressure variations, thus suggesting its potential application as a geobarometer for plagioclase peridotites.

REFERENCES

Baker, D. R. (2004). Piston-cylinder calibration at 400 to 500 MPa: A comparison of using water solubility in albite melt and NaCl melting. *American Mineralogist* **89**, 1553–1556.

Baker, M. B. & Stolper, E. M. (1994). Determining the composition of high-pressure mantle melts using diamond aggregates. *Geochimica et Cosmochimica Acta* **58**, 2811–2827.

Baker, M. B., Hirschmann, M. M., Ghiorso, M. S. & Stolper, E. M. (1995). Compositions of near-solidus peridotite melts from experiments and thermodynamic calculations. *Nature* **375**, 308–311.

Bodinier, J.-L. & Godard, M. (2003). Orogenic, ophiolitic and abyssal peridotites. In: Holland, H. D. & Turekian, K. K. (eds) *Treatise on Geochemistry*. Oxford: Elsevier.

Borghini, G. (2008). *The spinel- to plagioclase-facies transition in mantle peridotites: natural and experimental constraints*. PhD thesis, University of Genova.

Borghini, G., Rampone, E., Crispini, L., De Ferrari, R. & Godard, M. (2007). Origin and emplacement of ultramafic–mafic intrusions in the Erro–Tobbio mantle peridotite (Ligurian Alps, Italy). *Lithos* **94**, 210–229.

Canil, D., Johnston, S. T., Evers, K., Shellnutt, J. G. & Creaser, A. (2003). Mantle exhumation in an early Palaeozoic passive margin, northern Cordillera, Yukon. *Journal of Geology* **111**, 313–327.

Cannat, M. & Seyler, M. (1995). Transform tectonics, metamorphic plagioclase and amphibolitization in ultramafic rocks of the Vema transform fault (Atlantic Ocean). *Earth and Planetary Science Letters* **133**, 283–298.

Cannat, M., Sauter, D. & Mendel, V. (2006). Modes of seafloor generation at a melt-poor ultraslow-spreading ridge. *Geology* **34**, 605–608.

Chazot, G., Charpentier, S., Kornprobst, J. & Luais, B. (2005). Lithospheric mantle evolution during continental break-up: the west Iberia non-volcanic passive margin. *Journal of Petrology* **46**, 2527–2568.

Connolly, J. A. D. (1990). Calculation of multivariable phase diagrams: an algorithm based on generalized thermodynamics. *American Journal of Science* **290**, 666–718.

Connolly, J. A. D. & Petrini, K. (2002). An automated strategy for calculation of phase diagram sections and retrieval of rock properties as a function of physical conditions. *Journal of Metamorphic Geology* **20**, 697–708.

Dick, H. J. B. (1989). Abyssal peridotite, very slow spreading ridges and oceanic ridge magmatism. In: Saunders, A. D. & Norris, M. J. (eds) *Magmatism in the Ocean Basins. Geological Society, London, Special Publications* **42**, 71–105.

Dick, H. J. B. & Bullen, T. D. (1984). Chromian spinel as a petrogenetic indicator in abyssal and alpine-type peridotites and spatially associated lavas. *Contributions to Mineralogy and Petrology* **86**, 54–76.

Dijkstra, A. H., Drury, M. R. & Visser, L. R. M. (2001). Structural petrology of plagioclase peridotite in the West Othris mountains (Greece): melt impregnation in mantle lithosphere. *Journal of Petrology* **42**, 5–24.

Dijkstra, A. H., Barth, M. G., Martyn, R., Drury, R., Mason, P. R. D. & Visser, L. R. M. (2003). Diffuse porous melt flow and melt–rock reaction in the mantle lithosphere at a slow-spreading ridge: a structural petrology and LA-ICP-MS study of the Othris peridotite massif (Greece). *Geochemistry, Geophysics, Geosystems* **4**, Paper 2001GC000278.

Elthon, D. (1992). Chemical trends in abyssal peridotites: refertilization of depleted suboceanic mantle. *Journal of Geophysical Research* **97**, 9015–9025.

Fabries, J., Lorand, J.-P. & Bodinier, J.-P. (1998). Petrogenetic evolution of orogenic lherzolite massifs in the central and western Pyrenees. *Tectonophysics* **292**, 145–167.

Fallon, T. J. & Green, D. H. (1987). Anhydrous partial melting of MORB pyrolite and other peridotite compositions at 10 kbar; implications for the origin of primitive MORB glasses. *Mineralogy and Petrology* **37**, 181–219.

Fallon, T. J. & Green, D. H. (1988). Anhydrous partial melting of peridotite from 8 to 35 kbar and the petrogenesis of MORB. *Journal of Petrology, Special Lithosphere Issue* 379–414.

Fallon, T. J., Green, D. H., O'Neill, H. St. C. & Hibberson, W. O. (1997). Experimental tests of low degree peridotite partial melt compositions: implications for the nature of anhydrous near-solidus peridotite melts at 1 GPa. *Earth and Planetary Science Letters* **152**, 149–162.

Fallon, T. J., Green, D. H., Danyushevsky, L. V. & Faul, U. H. (1999). Peridotite melting at 1·0 and 1·5 GPa: an experimental evaluation of techniques using diamond aggregates and mineral mixes for determination of near-solidus melts. *Journal of Petrology* **40**, 1343–1375.

Fallon, T. J., Green, D. H., Danyushevsky, L. V. & McNeill, A. W. (2008). The composition of near-solidus partial melts of fertile peridotite at 1 and 1·5 GPa: implications for petrogenesis of MORB. *Journal of Petrology* **49**, 591–613.

Fumagalli, P. & Poli, S. (2005). Experimentally determined phase relations in hydrous peridotites to 6·5 GPa and their consequences on the dynamics of subduction zones. *Journal of Petrology* **45**, 1–24.

Furusho, M. & Kanagawa, K. (1999). Transformation-induced strain localization in a lherzolite mylonite from the Hidaka metamorphic belt of central Hokkaido, Japan. *Tectonophysics* **313**, 411–432.

Gasparik, T. (1984). Two-pyroxene thermobarometry with new experimental data in the system CaO–MgO–Al$_2$O$_3$–SiO$_2$. *Contributions to Mineralogy and Petrology* **87**, 87–97.

Gasparik, T. (1987). Orthopyroxene thermobarometry in simple and complex systems. *Contributions to Mineralogy and Petrology* **96**, 357–370.

Green, D. H. (1963). Alumina content of enstatite in a Venezuelan high temperature peridotite. *Geological Society of America Bulletin* **74**, 1397–1402.

Green, D. H. (1964). The petrogenesis of the high-temperature peridotite intrusion in the Lizard Area, Cornwall. *Journal of Petrology* **5**, 134–188.

Green, D. H. & Fallon, T. J. (1998). Pyrolite: A Ringwood concept and its current expression. In: Jackson, I. (ed.) *The Earth's Mantle.* Cambridge: Cambridge University Press, pp. 311–378.

Green, D. H. & Hibberson, W. (1970). The instability of plagioclase in peridotite at high pressure. *Lithos* **3**, 209–221.

Green, D. H. & Ringwood, A. E. (1970). Mineralogy of peridotitic compositions under upper mantle conditions. *Physics of the Earth and Planetary Interiors* **3**, 359–371.

Green, D. H., Hibberson, W. O. & Jaques, A. L. (1979). Petrogenesis of mid ocean ridge basalt. In: McElhinney, M. W. (ed.) *The Earth: its Origin, Structure and Evolution.* London: Academic Press, pp. 265–299.

Gudfinnsson, G. H. & Presnall, D. C. (2000). Melting behaviour of model lherzolite in the system CaO–MgO–Al$_2$O$_3$–SiO$_2$–FeO at 0·7–2·8 GPa. *Journal of Petrology* **41**, 1241–1269.

Hamilton, D. L. & Henderson, C. M. B. (1968). The preparation of silicate compositions by a gelling method. *Mineralogical Magazine* **36**, 832–838.

Hamlyn, P. R. & Bonatti, E. (1980). Petrology of mantle-derived ultramafic from the Owen fracture zone, northwest Indian Ocean: implications for the nature of the oceanic upper mantle. *Earth and Planetary Science Letters* **48**, 65–79.

Hellebrand, E., Snow, J. E. & Mühe, R. (2002). Mantle melting beneath Gakkel Ridge (Arctic Ocean): abyssal peridotite spinel compositions. *Chemical Geology* **182**, 227–235.

Hermann, J., O'Neill, H. S. C. & Berry, A. J. (2005). Titanium solubility in olivine in the system TiO$_2$–MgO–SiO$_2$: no evidence for an ultra-deep origin of Ti-bearing olivine. *Contributions to Mineralogy and Petrology* **148**, 746–760.

Herzberg, C. T. (1978). Pyroxene geothermometry and geobarometry: experimental and thermodynamic evaluation of some subsolidus phase relations involving pyroxenes in the system CaO–MgO–Al$_2$O$_3$–SiO$_2$. *Geochimica et Cosmochimica Acta* **42**, 945–957.

Holland, T. J. B. & Powell, R. (1998). An internally consistent thermodynamic data set for phases of petrological interest. *Journal of Metamorphic Geology* **16**, 309–343.

Hoogerduijn Strating, E. H., Rampone, E., Piccardo, G. B., Drury, M. R. & Vissers, R. L. M. (1993). Subsolidus emplacement of mantle peridotites during incipient oceanic rifting and opening of the Mesozoic Tethys (Voltri Massif, NW Italy). *Journal of Petrology* **34**, 901–927.

Jaques, A. L. & Green, D. H. (1980). Anhydrous melting of peridotite at 0–15 kb pressure and genesis of tholeiitic basalts. *Contributions to Mineralogy and Petrology* **73**, 287–310.

Kaczmarek, M. A. & Müntener, O. (2008). Juxtaposition of melt impregnation and high-temperature shear zones in the upper mantle; field and petrological constraints from the Lanzo peridotite (Northern Italy). *Journal of Petrology* **49**, 2187–2220.

Keshav, S., Tirone, M., Gudfinnsson, G. & Presnall, D. (2008). Melting in the system CaO–MgO–Al$_2$O$_3$–FeO–Cr$_2$O$_3$ spanning the plagioclase–spinel lherzolite transition at 7 to 10 kbar: experiments versus thermodynamics. EOS Transactions, American Geophysical Union 89(53), Fall Meeting Supplement, abstract.

Kinzler, R. J. (1997). Melting of mantle peridotite at pressures approaching the spinel to garnet transition: application to mid-ocean ridge basalt petrogenesis. *Journal of Geophysical Research* **102**, 853–874.

Klemme, S. (2004). The influence of Cr on the garnet–spinel transition in the Earth's mantle: experiments in the system MgO–Cr$_2$O$_3$–SiO$_2$ and thermodynamic modelling. *Lithos* **77**, 639–646.

Klemme, S. & O'Neill, H. St. C. (2000). The effect of Cr on the solubility of Al in orthopyroxene: experiments and thermodynamic modelling. *Contributions to Mineralogy and Petrology* **140**, 84–98.

Kornprobst, J. & Tabit, A. (1988). Plagioclase-bearing ultramafic tectonites from the Galicia margin (Leg 103, Site 637): comparison of their origin and evolution with low pressure ultramafic bodies in western Europe. In: Boillot, G., Winterer, E. L. *et al.* (eds)

Proceeding of the Ocean Drilling Program, Scientific Results, 103. College Station, TX: Ocean Drilling Program, pp. 253–263.

Kushiro, I. & Yoder, H. S., Jr (1966). Anorthite–forsterite and anorthite–enstatite reactions and their bearing on the basalt–eclogite transformation. *Journal of Petrology* **7**, 337–362.

Libourel, G. (1999). Systematics of calcium partitioning between olivine and silicate melt: implications for melt structure and calcium content of magmatic olivines. *Contributions to Mineralogy and Petrology* **136**, 63–80.

MacGregor, I. D. (1967). Mineralogy of model mantle composition. In: Wyllie, P. J. (ed.) *Ultramafic and Related Rocks*. New York: John Wiley, pp. 382–393.

McDonough, W. F. & Sun, S-s. (1995). The composition of the Earth. *Chemical Geology* **120**, 223–253.

Menzies, M. A. (1973). Mineralogy and partial melt textures within an ultramafic–mafic body, Greece. *Contributions to Mineralogy and Petrology* **42**, 273–285.

Montanini, A., Tribuzio, R. & Anczkiewicz, R. (2006). Exhumation history of a garnet pyroxenite-bearing mantle section from a continent–ocean transition (Northern Apennine ophiolites, Italy). *Journal of Petrology* **47**, 1943–1971.

Müntener, O. & Manatschal, G. (2006). High degrees of melt extraction recorded by spinel harzburgite of the Newfoundland margin: The role of inheritance and consequences for the evolution of the southern North Atlantic. *Earth and Planetary Science Letters* **252**, 437–452.

Müntener, O., Pettke, T., Desmours, L., Meier, M. & Schaltegger, U. (2004). Refertilization of mantle peridotite in embryonic ocean basins: trace element and Nd-isotope evidence and implications for crust–mantle relationships. *Earth and Planetary Science Letters* **221**, 293–308.

Müntener, O., Piccardo, G. B., Polino, R. & Zanetti, A. (2005). Revisiting the Lanzo peridotite (NW Italy): 'asthenospherization' of ancient mantle lithosphere. *Ofioliti* **30**, 111–124.

Newman, J., Lamb, W. M., Drury, M. R. & Vissers, R. L. M. (1999). Deformation processes in a peridotite shear zone: reaction-softening by an H_2O-deficient, continuous net transfer reaction. *Tectonophysics* **303**, 193–222.

Niida, K. & Green, D. H. (1999). Stability and chemical composition of pargasitic amphibole in MORB pyrolite under upper mantle conditions. *Contributions to Mineralogy and Petrology* **135**, 18–40.

Niu, Y. L. (2004). Bulk-rock major and trace element compositions of abyssal peridotites: implications for mantle melting, melt extraction and post-melting processes beneath mid-ocean ridges. *Journal of Petrology* **45**, 2423–2458.

Niu, Y. L., Langmuir, C. H. & Kinzler, R. J. (1997). The origin of abyssal peridotites: a new perspective. *Earth and Planetary Science Letters* **152**, 251–265.

Obata, M. (1976). The solubility of Al_2O_3 in orthopyroxenes in spinel and plagioclase peridotites and spinel pyroxenite. *American Mineralogist* **61**, 804–816.

Obata, M. (1980). The Ronda peridotite: garnet–spinel- and plagioclase-lherzolite and the P–T trajectories of a high-temperature mantle intrusion. *Journal of Petrology* **21**, 533–572.

O'Hara, M. J. (1967). Mineral paragenesis in ultrabasic rocks. In: Wyllie, P. J. (ed.) *Ultramafic and Related Rocks*. New York: John Wiley, pp. 393–402.

O'Neill, H. St. C. (1981). The transition between spinel lherzolite and garnet lherzolite, and its use as a geobarometer. *Contributions to Mineralogy and Petrology* **77**, 185–194.

Ozawa, K. & Takahashi, N. (1995). P–T history of a mantle diapir: the Horoman peridotite complex, Hokkaido, northern Japan. *Contributions to Mineralogy and Petrology* **120**, 223–248.

Piccardo, G. B. & Vissers, R. L. M. (2007). The pre-oceanic evolution of the Erro–Tobbio peridotite (Voltri Massif, Ligurian Alps, Italy). *Journal of Geodynamics* **43**, 417–449.

Piccardo, G. B., Messiga, B. & Vannucci, R. (1988). The Zabargad peridotite–pyroxenite association: petrological constraints on its evolution. *Tectonophysics* **150**, 135–162.

Piccardo, G. B., Müntener, O., Zanetti, A. & Pettke, T. (2004*a*). Ophiolitic peridotites of the Alpine–Apennine system: mantle processes and geodynamic relevance. *International Geology Review* **46**, 1119–1159.

Piccardo, G. B., Müntener, O., Zanetti, A., Romairone, A., Bruzzone, S., Poggi, E. & Spagnolo, G. (2004*b*). The Lanzo South peridotite: melt–peridotite interaction in the mantle lithosphere of the Jurassic Ligurian Tethys. *Ofioliti* **29**, 37–62.

Piccardo, G. B., Zanetti, A., Spagnolo, G. & Poggi, E. (2005). Recent researches on melt–rock interaction in the Lanzo South peridotite. *Ofioliti* **30**, 115–124.

Piccardo, G. B., Zanetti, A., Poggi, E., Spagnolo, G. & Müntener, O. (2007). Melt/peridotite interaction in the Lanzo South peridotite: field, textural and geochemical evidence. *Lithos* **94**, 181–209.

Presnall, D. C., Dixon, J. R., O'Donnell, T. H. & Dixon, S. A. (1979). Generation of mid-ocean ridge tholeiites. *Journal of Petrology* **20**, 3–35.

Presnall, D. C., Gudfinnsson, G. H. & Walter, M. J. (2002). Generation of mid-ocean ridge basalt at pressure from 1 to 7 GPa. *Geochimica et Cosmochimica Acta* **66**, 2073–2090.

Rampone, E. & Borghini, G. (2008). The melt intrusion/interaction history of the Erro–Tobbio peridotites (Ligurian Alps, Italy): Insights on mantle processes at non-volcanic passive margins. *European Journal of Mineralogy* **20**, 573–585.

Rampone, E., Piccardo, G. B., Vannucci, R., Bottazzi, P. & Ottolini, L. (1993). Subsolidus reactions monitored by trace element partitioning: the spinel- to plagioclase-facies transition in mantle peridotites. *Contributions to Mineralogy and Petrology* **115**, 1–17.

Rampone, E., Hofmann, A. W., Piccardo, G. B., Vannucci, R., Bottazzi, P. & Ottolini, L. (1995). Petrology, mineral and isotope geochemistry of the External Liguride peridotites (Northern Appennine, Italy). *Journal of Petrology* **36**, 61–76.

Rampone, E., Piccardo, G. B., Vannucci, R. & Bottazzi, P. (1997). Chemistry and origin of trapped melts in ophiolitic peridotites. *Geochimica et Cosmochimica Acta* **61**, 4557–4569.

Rampone, E., Romairone, A., Abouchami, W., Piccardo, G. B. & Hofmann, W. (2005). Chronology, petrology and isotope geochemistr of the Erro–Tobbio peridotites (Ligurian Alps, Italy): records of late Palaeozoic lithospheric extension. *Journal of Petrology* **46**, 799–827.

Rampone, E., Piccardo, G. B. & Hofmann, A. W. (2008). Multi-stage melt–rock interaction in the Mt. Maggiore (Corsica, France) ophiolitic peridotites: microstructural and geochemical records. *Contributions to Mineralogy and Petrology* **156**, 453–475.

Schreiber, H. D. & Haskin, L. A. (1976). Chromium in basalts: experimental determination of redox states and partitioning among silicate phases. *Proceedings of the 7th Lunar Science Conference. Geochimica et Cosmochimica Acta Supplement* 1221–1259.

Seyler, M. & Bonatti, E. (1997). Regional-scale melt–rock interaction in lherzolitic mantle in the Romanche fracture zone (Atlantic Ocean). *Earth and Planetary Science Letters* **146**, 273–287.

Simon, N. S. C. & Podladchikov, Y. Y. (2008). The effect of mantle composition on density in the extending lithosphere. *Earth and Planetary Science Letters* **272**, 148–157.

Takazawa, E., Frey, F., Shimizu, N. & Obata, M. (1996). Evolution of the Horoman peridotite (Hokkaido, Japan): implications from pyroxene compositions. *Chemical Geology* **134**, 3–26.

Tartarotti, P., Susini, S., Nimis, P. & Ottolini, L. (2002). Melt migration in the upper mantle along the Romanche fracture zone (Equatorial Atlantic). *Lithos* **63**, 125–149.

Ulmer, P. & Luth, R. W. (1991). The graphite fluid equilibrium in P, T, fO$_2$ space: an experimental determination to 30 kbar and 1600°C. *Contributions to Mineralogy and Petrology* **106**, 265–272.

Walter, M. J. (1998). Melting of garnet peridotite and the origin of komatiite and depleted lithosphere. *Journal of Petrology* **39**, 29–60.

Walter, M. J. & Presnall, D. C. (1994). Melting behaviour of simplified lherzolite in the system CaO–MgO–Al$_2$O$_3$–SiO$_2$–Na$_2$O from 7 to 35 kbar. *Journal of Petrology* **35**, 329–359.

Wasylenki, L. E., Baker, M. B., Kent, A. J. R. & Stolper, E. M. (2003). Near-solidus melting of the shallow upper mantle: partial melting experiments on deplets peridotite. *Journal of Petrology* **44**, 1163–1191.

Webb, S. A. C. & Wood, B. J. (1986). Spinel–pyroxene–garnet relationships and their dependence on Cr/Al ratio. *Contributions to Mineralogy and Petrology* **92**, 471–480.

Wood, B. J. & Yuen, D. A. (1983). The role of lithospheric phase transitions on seafloor flattening at old ages. *Earth and Planetary Science Letters* **66**, 303–314.

Woodland, A. B., Kornprobst, J. & Wood, B. (1992). Oxygen thermobarometry of orogenic lherzolite massifs. *Journal of Petrology* **33**, 203–230.